Models for Iron-Oxo Proteins. Structures and Properties of $Fe^{II}Fe^{III}$, $Zn^{II}Fe^{III}$, and $Fe^{II}Ga^{III}$ Complexes with (μ-Phenoxo)bis(μ-carboxylato)dimetal Cores

A. S. Borovik,[†] Vasilios Papaefthymiou,[⊥] Lucille F. Taylor,[‡] Oren P. Anderson,*[,‡] and Lawrence Que, Jr.*[,†]

Contribution from the Department of Chemistry, University of Minnesota, Minneapolis, Minnesota 55455, Department of Chemistry, Colorado State University, Fort Collins, Colorado 80523, and Gray Freshwater Biological Institute, University of Minnesota, Navarre, Minnesota 55392. *Received December 12, 1988*

Abstract: A series of bimetallic complexes, $[M^{II}M'^{III}BPMP(O_2CR)_2]X_2$ where BPMP is the anion of 2,6-bis[(bis(2-pyridylmethyl)amino)methyl]-4-methylphenol, has been synthesized to provide models for binuclear metal-oxo centers in proteins (**1**, M = M' = Fe, R = C_2H_5, X = BPh_4; **2**, M = M' = Fe, R = C_6H_5, X = PF_6; **3**, M = Fe, M' = Ga, R = C_2H_5, X = BPh_4; **4**, M = Zn, M' = Fe, R = CH_3, X = BPh_4; **5**, M = Zn, M' = Fe, R = C_2H_5, X = BPh_4). The complexes **1'** (**1**·CH_3COCH_3·0.5CH_3CN) and **4'** (**4**·CH_3CN) have been characterized by X-ray diffraction methods as having (μ-phenoxo)bis(μ-carboxylato)dimetal cores. Both **1'** and **4'** crystallize in the triclinic space group $P\bar{1}$ with the following unit cell parameters: for **1'**, a = 13.489 (9) Å, b = 13.514 (6) Å, c = 25.258 (15) Å, α = 77.23 (4)°, β = 77.89 (5)°, γ = 61.43 (4)°, and Z = 2; for **4'**, a = 12.914 (4) Å, b = 14.991 (3) Å, c = 20.736 (6) Å, α = 101.66 (2)°, β = 106.84 (2)°, γ = 100.19 (2)°, and Z = 2. The metal centers in the mixed valence complex **1'** are ordered as indicated by the differences in the Fe-O bond lengths; these match well with Fe^{III}-O and Fe^{II}-O bond lengths in complexes of established structure and valence. The metal centers in **4'** exhibit differences in Fe-O and Zn-O bond lengths, but the crystallographic analysis suggests the presence of some disorder in the metal occupancies in this case. The $Fe^{II}Fe^{III}$ complexes have been characterized by electronic spectral, Mössbauer, EPR, NMR, and electrochemical methods. The assignment of these properties to the individual iron centers is facilitated by the availability of the analogous heterobimetallic complexes wherein one of the paramagnetic centers in the mixed valence complex is replaced with a diamagnetic center of corresponding charge, i.e., Zn^{II} for Fe^{II} or Ga^{III} for Fe^{III} Thus, **1** exhibits electronic spectral features near 385, 554, and 1350 nm, assigned to Fe^{II}-to-pyridine, phenolate-to-Fe^{III}, and intervalence charge-transfer transitions, respectively. Its NMR spectrum exhibits sharp, isotropically shifted resonances, which number half of that expected for a valence-trapped species; this indicates that electron transfer between the metal centers is fast on the NMR time scale under ambient conditions. Its Mossbauer spectrum at temperatures below 200 K, on the other hand, shows features indicative of trapped valences. Taken together, the NMR, Mossbauer, and electronic spectral data classify **1** as a class II mixed valence complex in the Robin-Day scheme. In contrast, the valences appear trapped in the solid state, even at room temperature, as indicated by crystallographic and Mössbauer data. **1** exhibits reversible one-electron waves at +692 and -10 mV versus SCE, corresponding to the $Fe^{III}Fe^{III}/Fe^{II}Fe^{III}$ and $Fe^{II}Fe^{III}/Fe^{II}Fe^{II}$ couples, respectively. The high potential of the first wave, which is also observed for the corresponding $Fe^{II}Ga^{III}$-bis(propionate) and $Mn^{II}Mn^{III}$-bis(acetate) complexes, emphasizes the point that the BPMP/bis(carboxylate) ligand combination appears to stabilize a total metal charge of +5. Lastly, **1** exhibits a broad EPR signal centered near g = 1.6, which is not observed in either the analogous $Zn^{II}Fe^{III}$ or $Fe^{II}Ga^{III}$ complexes. This signal is similar to those observed for the mixed valence forms of binuclear iron-oxo proteins.

In recent years, binuclear iron-oxo centers have emerged as a common structural component in the active sites of several metalloproteins.[1] These centers have important functional roles in hemerythrin,[2] ribonucleotide reductase,[3] methane monooxygenase,[4] and the purple acid phosphatases.[5] The binuclear centers in such proteins are known or are postulated to exist in either an oxidized ($Fe^{III}Fe^{III}$), a reduced ($Fe^{II}Fe^{II}$), or a mixed valence ($Fe^{II}Fe^{III}$) form. The prototype and best characterized member of this class of proteins is hemerythrin (Hr), a respiratory protein found in some marine invertebrates. In particular, the $Fe^{III}Fe^{III}$ form has been shown by crystallographic and spectroscopic studies to have a (μ-oxo)bis(μ-carboxylato)diiron core.[1,2,6] This structure has been reproduced in synthetic $Fe^{III}Fe^{III}$ complexes by spontaneous self-assembly methods, thus illustrating the thermodynamic stability of this triply bridged binuclear unit.[7] Diiron complexes of this type have served as excellent models for the structural and spectroscopic properties of the oxidized form of binuclear iron proteins.

The structures of the diiron centers in the reduced and mixed valence forms are less well understood. For deoxyhemerythrin (deoxyHr), a variety of physical measurements suggest that the triply bridged unit is retained, with the oxo group being protonated to give a (μ-hydroxo)bis(μ-carboxylato)diiron(II,II) core.[1,8,9] It appears that this structure may also be present in the $Fe^{II}Fe^{III}$ (semimet) forms of hemerythrin,[10] which can be generated either from the oxidation of deoxyHr or reduction of metHr,[11] yet efforts

[†] University of Minnesota, Minneapolis.
[‡] Colorado State University.
[⊥] University of Minnesota, Navarre.

(1) (a) Que, L., Jr.; Scarrow, R. C. In *Metal Clusters in Proteins*; Que, L., Jr., Ed.; ACS Symposium Series 372; American Chemical Society: Washington DC, 1988; pp 159-178. (b) Lippard, S. J. *Angew. Chem., Intl. Ed. Engl.* **1988**, *27*, 344-361.
(2) Wilkins, P. C.; Wilkins, R. G. *Coord. Chem. Rev.* **1987**, *79*, 195-214.
(3) Reichard, P.; Ehrenberg, A. *Science (Washington, D.C.)* **1983**, *221*, 514-519.
(4) (a) Woodland, M. P.; Patil, D. S.; Cammack, R.; Dalton, H. *Biochim. Biophys. Acta* **1986**, *873*, 237-242. (b) Prince, R. C.; George, G. N.; Savas, J. C.; Cramer, S. P.; Patel, R. N. *Biochim. Biophys. Acta* **1988**, *952*, 220-229. (c) Ericson, A.; Hedman, B.; Hodgson, K. O.; Green, J.; Dalton, H.; Bentsen, J. G.; Beer, R. H.; Lippard, S. J. *J. Am. Chem. Soc.* **1988**, *110*, 2330-2332. (d) Fox, B. G.; Surerus, K. K.; Münck, E.; Lipscomb, J. D. *J. Biol. Chem.* **1988**, *263*, 10553-10556.
(5) (a) Antanaitis, B. C.; Aisen, P. *Adv. Inorg. Biochem.* **1983**, *5*, 111-136. (b) Averill, B. A.; Davis, J. C.; Burman, S.; Zirino, T.; Sanders-Loehr, J.; Loehr, T. M.; Sage, J. T.; Debrunner, P. G. *J. Am. Chem. Soc.* **1987**, *109*, 3760-3767.
(6) (a) Stenkamp, R. E.; Sieker, L. C.; Jensen, L. H. *J. Am. Chem. Soc.* **1984**, *106*, 618-622. (b) Sheriff, S.; Hendrickson, W. A.; Smith, J. L. *J. Mol. Biol.* **1987**, *197*, 273-296.
(7) (a) Armstrong, W. H.; Spool, A.; Papaefthymiou, G. C.; Frankel, R. B.; Lippard, S. J. *J. Am. Chem. Soc.* **1984**, *106*, 3653-3667. (b) Wieghardt, K.; Pohl, K.; Gebert, W. *Angew. Chem., Intl. Ed. Engl.* **1983**, *22*, 727-728. (c) Spool, A.; Williams, I. D.; Lippard, S. J. *Inorg. Chem.* **1985**, *24*, 2156-2162. (d) Toftlund, H.; Murray, K. S.; Zwack, P. R.; Taylor, L. F.; Anderson, O. P. *J. Chem. Soc., Chem. Commun.* **1986**, 191-193. (e) Gomez-Romero, P.; Casan-Pator, N.; Ben-Hussein, A.; Jameson, G. *J. Am. Chem. Soc.* **1988**, *110*, 1988-1990.
(8) Zhang, K.; Stern, E. A.; Ellis, F.; Sanders-Loehr, J.; Shiemke, A. K. *Biochemistry* **1988**, *27*, 7470-7479.

0002-7863/89/1511-6183$01.50/0

to obtain conclusive structural results for semimethemerythrins have been hampered because of their thermodynamic instability. The semimethemerythrins have distinct EPR signals with $g_{av} \approx 1.8$,[11] as do corresponding forms of methane monooxygenase[4a,d] and purple acid phosphatase.[5] The g_{av} value of <2 is characteristic of mixed valence diiron centers in proteins and is indicative of antiferromagnetic coupling between the Fe^{II} and Fe^{III} centers. It has been proposed that the mixed valence forms of these proteins may be involved in protein function. For example, the mechanism of O_2 binding to hemerythrin is postulated to go through a mixed valence intermediate,[12] and the active form of the mammalian purple acid phosphatases is the $Fe^{II}Fe^{III}$ derivative.[5] It is apparent that more studies into the structure and physical properties of such sites are necessary before we can obtain a clear understanding of how these binuclear centers can have vastly different functions.

As part of our effort to probe the properties of biologically important mixed valence centers, we have undertaken a study aimed at developing the coordination chemistry of triply bridged $Fe^{II}Fe^{III}$ complexes. Recently, four examples of binuclear mixed valence iron complexes, which are postulated to have triply bridged cores, have been reported, but none are structurally characterized.[13-15] We have approached the synthesis of such $Fe^{II}Fe^{III}$ complexes by using a binucleating ligand strategy (as have Suzuki et al.[13]), and for the present study we have employed the symmetrical binucleating ligand 2,6-bis[(bis(2-pyridylmethyl)amino)methyl]-4-methylphenol, HBPMP.[16,17] This ligand has the advantage of holding the two metal ions in close proximity through a phenoxo bridge while preventing the $Fe^{II}Fe^{III}$ complex from disproportionating in solution, a problem that has hindered the characterization of mixed valence species derived from μ-oxodiiron(III) complexes.[7a,15] Thus, stable mixed valence complexes with (μ-phenoxo)bis(μ-carboxylato)diiron(II,III) cores have been prepared.[15,18]

During the course of this study, we discovered a general synthetic route for preparing heterobimetallic complexes in which one of the metal ions is iron. These complexes also contain (μ-phenoxo)bis(μ-carboxylato)dimetal cores.[19] The $Zn^{II}Fe^{III}$ and $Fe^{II}Ga^{III}$ complexes, in particular, have proven useful in probing the physical properties of the individual iron sites in our $Fe^{II}Fe^{III}$ complexes. Hence, this paper presents the structural and physical properties of the bis(carboxylato)-bridged $Fe^{II}Fe^{III}$, $Zn^{II}Fe^{III}$, and $Fe^{II}Ga^{III}$ complexes of HBPMP. The X-ray analysis of $[Fe^{II}Fe^{III}BPMP(OPr)_2](BPh_4)_2$, **1**, represents the first example of a structurally well-characterized triply bridged $Fe^{II}Fe^{III}$ complex, while that of $[Zn^{II}Fe^{III}BPMP(OPr)_2](BPh_4)_2$, **4**, demonstrates that the heterobimetallic series of complexes also exhibit the triply bridged core. Preliminary accounts of these results have previously been reported.[18,19]

Experimental Section

All reagents and solvents were purchased from commercial sources and used as received, unless noted otherwise. The following solvents were distilled under nitrogen before use: tetrahydrofuran (THF) from sodium benzophenone ketyl, methanol from $Mg(OCH_3)_2$, and acetonitrile from CaH_2. Melting points were obtained with the use of an Electrothermal apparatus and are uncorrected. Flash chromatography was performed according the general procedure of Still.[20] Analytical thin-layer chromatography was done using Polygram precoated silica gel or alumina (neutral) plates. Microanalyses were performed by Desert Analytics, Inc., Tucson, AZ.

2,6-Bis(chloromethyl)-4-methylphenol.[21] 2,6-Bis(hydroxymethyl)-4-methylphenol[21] (5.0 g, 30 mmol) in 25 mL of methylene chloride was added to a solution of 14 g (120 mmol) of thionyl chloride in 50 mL of methylene chloride. After stirring for 24 h, the mixture was poured over 50 mL of ice and made neutral (pH $\approx$ 7) with aqueous NaOH. The aqueous solution was extracted with three 50-mL portions of methylene chloride, washed with brine, and dried over anhydrous Na_2SO_4. The dried solution was evaporated to dryness at reduced pressure, and 5.7 g (92%) of the product was obtained as a pale-yellow solid, which was used without further purification: mp 83–84 °C [lit. mp 87 °C]; ^1H NMR δ ($CDCl_3$, 200 MHz) 2.28 (s, 3 H, $ArCH_3$), 4.66 (s, 4 H, $ArCH_2Cl$), 7.09 (s, 2 H, ArH).

2,6-Bis[(bis(2-pyridylmethyl)amino)methyl]-4-methylphenol, HBPMP. This compound was synthesized by the literature method with the following modifications.[16] Under a dinitrogen atmosphere, a mixture of bis(2-pyridylmethyl)amine (6.8 g, 34 mmol) and triethylamine (6.9 g, 68 mmol) in 15 mL of THF was added dropwise to a stirred THF solution of 2,6-bis(chloromethyl)-4-methylphenol (3.5 g, 17 mmol) at 0 °C. When the addition was completed, the resulting mixture was allowed to warm to room temperature. After 4 days, the stirred mixture was filtered to remove the triethylammonium salts, and the filtrate was concentrated under reduced pressure. The residue was dissolved in 50 mL of water, and the product was extracted with three 50-mL portions of methylene chloride. The extracts were combined, washed with brine, and dried over anhydrous Na_2SO_4. The product was purified by flash chromatography employing acetone as the eluent to afford 3.0 g (33%) of a pale-yellow oil: ^1H NMR δ ($CDCl_3$) 2.22 (s, 3 H, $ArCH_3$), 3.77 (s, 4 H, $ArCH_2N$), 3.84 (s, 8 H, NCH_2py), 6.98 (s, 2 H, ArH), 7.10 (t, J = 5 Hz, 4 H, pyH), 7.55 (m, 8 H, pyH), 8.50 (d, J = 4 Hz, 4 H, pyH).

Bis(μ-propionato-O,O')(2,6-bis[(bis(2-pyridylmethyl)amino)-methyl]-4-methylphenolato)diiron(II,III) Bis(tetraphenylborate), $[Fe^{II}Fe^{III}BPMP(OPr)_2](BPh_4)_2 \cdot CH_3COCH_3$ (1). Method A. A solution of 0.14 g (0.26 mmol) of HBPMP in 10 mL of methanol was treated with a solution of 0.21 g (0.53 mmol) of $Fe(NO_3)_3 \cdot 9H_2O$ in 5 mL of methanol to yield a dark-green solution. Addition of 0.064 g (0.66 mmol) of sodium propionate in 3 mL of methanol caused the formation of a dark-gray solution. Metathesis with sodium tetraphenylborate (0.36 g, 1.1 mmol) resulted in the immediate precipatation of the crude product, which was filtered through a medium-fritted glass filter. Further purification was achieved by recrystallization of the crude product by vapor diffusion of methanol into an acetone solution of **1** to afford dark crystals of **1**. Diffraction quality crystals were obtained by the vapor diffusion of methanol into an acetonitrile/acetone solution of **1**; these crystals (hereafter referred to as **1'**) contained a molecule of occluded acetone and half a molecule of occluded acetonitrile. Anal. Calcd for $C_{90}H_{89}B_2Fe_2N_6O_6$ (**1**): C, 72.83; H, 6.06; N, 5.66. Found: C, 72.67; H, 5.93; N, 5.83. ^1H NMR δ (CD_3COCD_3) 3.83 (s, 2 H, pyH), 5.29 (s, 2 H, pyH), 12.93 (s, 2 H, NCH_2py), 18.74 (s, 6 H, $OPrCH_3$), 42.0 (s, 2 H, NCH_2py), 51.1 (s, 2 H, $OPrCH_2$), 54.4 (s, 2 H, pyH), 63.0 (s, 2 H, m-ArH), 67.7 (s, 2 H, pyH), 71.5 (s, 2 H, $OPrCH_2$), 72.1 (s, 3 H, p-$ArCH_3$), 73.4 (s, 2 H, pyH), 79.9 (s, 2 H, pyH), 107 (s, 2 H, NCH_2Ar), 163 (s, 2 H, pyH), 184 (s, 2 H, NCH_2py), 199 (s, 2 H, pyH), 262 (s, 2 H, NCH_2py), 377 (s, 2 H, NCH_2Ar).

Method B. A solution of HBPMP (0.337 g, 0.635 mmol) in 15 mL of methanol was treated with a solution of $Fe(NO_3)_3 \cdot 9H_2O$ (0.257 g, 0.635 mmol) in 5 mL of methanol to yield a dark-blue solution, which contains the mononuclear iron complex. Sequential addition of 0.214 g (0.635 mmol) of $Fe(BF_4)_2 \cdot 6H_2O$ in 5 mL of methanol, 0.244 g (2.54 mmol) of sodium propionate in 5 mL of methanol, and a methanolic solution of sodium tetraphenylborate (0.87 g, 2.5 mmol) afforded the crude product, which was filtered and purified as described in method A. Dark-gray crystals were obtained after recrystallization, affording 0.526 g (56%) of **1**. Mixed metal complexes may be synthesized with

(9) Reem, R. C.; Solomon, E. I. *J. Am. Chem. Soc.* **1987**, *109*, 1216–1226.
(10) Scarrow, R. C.; Maroney, M. J.; Palmer, S. M.; Que, L., Jr.; Roe, A. L.; Salowe, S. P.; Stubbe, J. *J. Am. Chem. Soc.* **1987**, *109*, 7857–7864.
(11) Muhoberac, B. B.; Wharton, D. C.; Babcock, L. M.; Harrington, P. C.; Wilkins, R. G. *Biochim. Biophys. Acta* **1980**, *626*, 337–345.
(12) Stenkamp, R. E.; Sieker, L. C.; Jensen, L. H.; McCallum, J. D.; Sanders-Loehr, J. *Proc. Natl. Acad. Sci. U.S.A.* **1985**, *82*, 713–716.
(13) (a) Suzuki, M.; Uehara, A.; Oshio, H.; Endo, K.; Yanaga, M.; Kida, S.; Saito, K. *Bull. Chem. Soc. Jpn.* **1987**, *60*, 3547–3555. (b) Suzuki, M.; Murata, S.; Uehara, A.; Kida, S. *Chem. Lett.* **1987**, 281–284. (c) Suzuki, M.; Uehara, A.; Endo, K. *Inorg. Chim. Acta* **1986**, *123*, L9–L10. (d) Suzuki, M.; Oshio, H.; Uehara, A.; Endo, K.; Yanaga, M.; Kida, S.; Saito, K. *Bull. Chem. Soc. Jpn.* **1988**, *61*, 3907–3913.
(14) Borovik, A. S.; Murch, B. P.; Que, L., Jr.; Papaefthymiou, V.; Münck, E. *J. Am. Chem. Soc.* **1987**, *109*, 7190–7191.
(15) Hartman, J. R.; Rardin, R. L.; Chaudhuri, P.; Pohl, K.; Wieghardt, K.; Nuber, B.; Weiss, J.; Papaefthymiou, G. C.; Frankel, R. B.; Lippard, S. J. *J. Am. Chem. Soc.* **1987**, *109*, 7387–7396.
(16) Suzuki, M.; Kanatomi, H.; Murase, I. *Chem. Lett., Chem. Soc. Jpn.* **1981**, 1745–1748.
(17) Abbreviations: HBPMP, 2,6-bis[(bis(2-pyridylmethyl)amino)-methyl]-4-methylphenol; OPr, propionate; $HBpz_3$, hydrotris(pyrazolyl)borate; OAc, acetate; Me_3TACN, 1,4,7-trimethyl-1,4,7-triazacyclononane; SCE, standard calomel electrode; $TBABF_4$, tetrabutylammonium tetrafluoroborate; HXTA, *N,N'*-(2-hydroxy-5-methyl-1,3-xylylene)bis(*N*-(carboxymethyl)-glycine).
(18) Borovik, A. S.; Que, L., Jr. *J. Am. Chem. Soc.* **1988**, *110*, 2345–2347.
(19) Borovik, A. S.; Que, L., Jr.; Papaefthymiou, V.; Münck, E.; Taylor, L. F.; Anderson, O. P. *J. Am. Chem. Soc.* **1988**, *110*, 1986–1988.
(20) Still, W. C.; Kahn, M.; Mitra, A. *J. Org. Chem.* **1978**, *43*, 2923–2925.
(21) Ullman, F.; Brittner, K. *Chem. Ber.* **1909**, *42*, 2523–2925.

this method by using other metal salts in place of $Fe(BF_4)_2$ (vide infra).

Bis(μ-benzoato-*O*,*O*′)(2,6-bis[(bis(2-pyridylmethyl)amino)methyl]-4-methylphenolato)diiron(II,III) Bis(hexafluorophosphate), $[Fe^{II}Fe^{III}BPMP(OBz)_2](PF_6)_2$ (2). This complex was prepared by using the same experimental procedure outlined in method A for **1**, with the following modifications. Sodium benzoate was used in place of sodium propionate, and the complex was metathesized with ammonium hexafluorophosphate and recrystallized from hot/cold methanol. Anal. Calcd for $C_{47}H_{43}F_{12}Fe_2N_6O_5P_2$ (**2**): C, 48.10; H, 3.70; N, 7.16. Found: C, 47.93; H, 3.83; N, 7.01. ^1H NMR δ (CD_3COCD_3) 4.47 (s, 2 H, pyH), 4.69 (s, 2 H, pyH), 14.1, 17.1, 42.8 (s, 2 H, NCH_2py), 53.9 (s, 2 H, pyH), 63.9 (s, 2 H, *m*-ArH), 67.7 (s, 2 H, pyH), 71.9 (s, 2 H, *p*-$ArCH_3$), 73.0 (s, 2 H, pyH), 79.4 (s, 2 H, pyH), 106 (s, 2 H, NCH_2Ar), 160 (s, 2 H, pyH), 187 (s, 2 H, NCH_2py), 198 (s, 2 H, pyH), 265 (s, 2 H, NCH_2py), 396 (s, 2 H, NCH_2Ar).

Bis(μ-propionato-*O*,*O*′)(2,6-bis[(bis(2-pyridylmethyl)amino)methyl]-4-methylphenolato)iron(II)gallium(III) Bis(tetraphenylborate), $[Fe^{II}Ga^{III}BPMP(OPr)_2](BPh_4)_2 \cdot CH_3COCH_3$ (3). This complex was prepared using $Ga(NO_3)_3 \cdot H_2O$ as the gallium(III) precursor and by employing method B described above for **1**, with the following modifications: after the crude product was isolated, it was initially purified by column chromatography on neutral alumina with acetone as the eluent. The yellow solution was collected and concentrated under reduced pressure. The resulting solid was dissolved in acetone and recrystallized by vapor diffusion of methanol into an acetone solution of **3**. Anal. Calcd for $C_{90}H_{89}B_2FeGaN_6O_6$ (**3**): C, 72.16; H, 6.00; N, 5.61. Found: C, 71.99; H, 6.01; N, 5.60. ^1H NMR δ (CD_3COCD_3) −1.23 (s), −0.526 (s), 3.77 (s), 4.90 (s), 5.08 (s), 5.37 (s), 5.82 (s), 6.53 (s), 7.62 (s), 8.33 (s), 9.47 (s), 10.2 (s), 11.8 (s), 13.2 (s), 15.9 (s), 19.2 (s), 19.4 (s), 19.6 (s), 35.0 (br), 36.5 (s), 42.6 (br), 44.6 (s), 45.6 (s), 53.0 (s), 63.7 (s), 98.6 (s), 108 (s), 125 (s), 185 (s), 239 (s).

Bis(μ-acetato-*O*,*O*′)(2,6-bis[(bis(2-pyridylmethyl)amino)methyl]-4-methylphenolato)zinc(II)iron(III) Bis(tetraphenylborate), $[Zn^{II}Fe^{III}BPMP(OAc)_2](BPh_4)_2 \cdot H_2O$ (4). This complex was synthesized following the procedure outlined in method B for **1**, using $Zn(OAc)_2 \cdot 2H_2O$ as the zinc(II) precursor and sodium acetate instead of sodium propionate. Dark-purple crystals were isolated, affording 0.318 g (58%) of **4**. Crystals (roughly triangular plates) suitable for the X-ray diffraction experiment were obtained by the vapor diffusion of methanol into a solution of **4** in acetonitrile/acetone. Those crystals (hereafter referred to as compound **4′**) were found to contain a molecule of occluded acetonitrile (vide infra). Anal. Calcd for $C_{85}H_{81}B_2FeN_6O_6Zn$ (**4**): C, 71.62; H, 5.74; N, 5.89. Found: C, 71.54; H, 5.71; N, 5.82. ^1H NMR δ (CD_3COCD_3) 17 (br), 44 (br), 63 (br), 74 (br).

Bis(μ-propionato-*O*,*O*′)(2,6-bis[(bis(2-pyridylmethyl)amino)methyl]-4-methylphenolato)zinc(II)iron(III) Bis(tetraphenylborate), $[Zn^{II}Fe^{III}BPMP(OPr)_2](BPh_4)_2 \cdot CH_3COCH_3$ (5). This compound was prepared as reported for **1** by the procedure described in method B. Zinc bromide was used as the zinc(II) precursor, which yielded 0.325 g (60%) of dark-purple crystals. Anal. Calcd for $C_{90}H_{89}B_2FeN_6O_6Zn$ (**5**): C, 72.37; H, 6.02; N, 5.63. Found: C, 72.41; H, 6.01; N, 5.63. ^1H NMR δ (CD_3COCD_3) 14 (br), 18 (br), 43 (br), 49 (br), 71 (br).

Crystallographic Results for $[Fe^{II}Fe^{III}BPMP(OPr_2)_2](BPh_4)_2 \cdot CH_3COCH_3 \cdot 0.5CH_3CN$, 1′. A crystal of **1′** was mounted on an Enraf-Nonius CAD4 diffractometer. Crystal data, together with the details of the diffraction experiment and subsequent calculations, are listed in Table I. The cell dimensions were obtained by least-squares refinement of the setting angles for 25 reflections (2θ = 15–28°). The stability of the crystal was monitored during data collection by measuring the intensities of three control reflections after every 4000 s of exposure time. No significant trend in these intensities was observed during the course of data acquisition. Lorentz and polarization corrections were applied to the data, and absorption corrections based on ψ scans were carried out (correction factors 0.975–1.000).

The structure was solved by using Patterson and Fourier methods. Neutral-atom scattering factors (including anomalous scattering) were used.[22] All non-H atoms were refined with anisotropic thermal parameters. Hydrogen atoms were included in calculated positions (C–H = 0.95 Å, B_H = 3.0). Weighted ($w = [\sigma^2(R) + gF^2]^{-1}$) least-squares refinement on F was carried out by alternately refining the cation or the anions plus solvent molecules until the largest shift/esd ratio was equal to 0.02. In the final ΔF map, the highest peak (0.82 e Å^{-3}) was located near the disordered CH_3CN solvate.

The final fractional atomic coordinates for **1′** are contained in Table II, while bond lengths and angles for the dinuclear complex cation are reported in Table III. A complete listing of bond lengths and angles, thermal parameters, hydrogen atom coordinates, and F_o/F_c tables has been supplied as supplementary material. The structure of the cation is shown in Figure 1a, together with the numbering scheme for the complex.

(22) *International Tables for X-Ray Crystallography*; Kynoch Press: Birmingham, England, 1969; Vol. IV, pp 55, 99, 149.

Table I. Crystallographic Experiments and Computations

compd	**1′**	**4′**
formula	$C_{91}H_{90.5}B_2Fe_2N_{6.5}O_6$	$C_{87}H_{82}B_2FeN_7O_5Zn$
formula wt, amu	1504.6	1448.5
temp, K	182	146
crystal system	triclinic	triclinic
space group	$P\bar{1}$	$P\bar{1}$
a, Å	13.489 (9)	12.914 (4)
b, Å	13.514 (6)	14.991 (3)
c, Å	25.258 (15)	20.736 (6)
α, deg	77.23 (4)	101.66 (2)
β, deg	77.89 (5)	106.84 (2)
γ, deg	61.43 (4)	100.19 (2)
V, Å^3	3914	3642
Z	2	2
F(000)	1584	1518
D(calc), g cm^{-3}	1.28	1.34
crystal dim, mm	0.25 × 0.10 × 0.35	0.38 × 0.20 × 0.56
radiation	Mo Kα (λ = 0.7107 Å)	Mo Kα
monochromator	graphite	graphite
μ, cm^{-1}	4.26	5.94
scan type	ω	Wyckoff
2θ range, deg	4–50	4–50
indices collected	$+h,\pm k,\pm l$	$+h,\pm k,\pm l$
reflections	13 728	13 462 measd
	12 838 unique	
	9531 used ($I > \sigma(I)$)	11 105 used ($I > 2.5\sigma(I)$)
scan spd, deg min^{-1}	2.4–12	4–29.30
no. of least-sq param	479	604
data/param	19.9	18.4
R[a]	0.055	0.070
R_w[a]	0.059	0.095
GOF[a]	1.25	1.83
g	5.9 × 10^{-8}	1.37 × 10^{-3}
slope, norm prob plot[b]	not determined	1.56

[a] $R = (\sum||F_o| - |F_c||)/(\sum|F_o|)$; $R_w = [(\sum w(|F_o| - |F_c|)^2)/(\sum w(F_o)^2)]^{1/2}$; GOF = $[(\sum w(|(F_o| - |F_c|)|)^2)/(N_{data} - N_{params})]^{1/2}$. [b] Abrahams, S. C. *Acta Crystallogr.* **1974**, *B30*, 261–268.

Crystallographic Results for $[Zn^{II}Fe^{III}BPMP(OAc)_2](BPh_4)_2 \cdot CH_3CN$, 4′. A crystal of **4′** was centered on a Nicolet R3m diffractometer. Crystal data, together with the details of the diffraction experiment and subsequent calculations, are listed in Table I. The cell dimensions were obtained by least-squares refinement of the setting angles for 25 reflections ($2\theta_{av}$ = 23.54°). Axial photographs about a, b, and c confirmed the lengths and symmetry of the axes. The stability of the crystal was monitored during data collection by measuring the intensities of three control reflections (500, 050, 005) every 97 data points. No significant trend in these intensities was observed during the course of data acquisition. Lorentz and polarization corrections were applied to the data, but no absorption correction was carried out, due to the small absorption coefficient.

The structure was solved by using the direct methods routine SOLV (SHELXTL program package written by G. M. Sheldrick and supplied by Nicolet XRD). Neutral-atom scattering factors (including anomalous scattering) were used.[22] In the penultimate ΔF map, an occluded molecule of CH_3CN appeared, identifying the crystal as **4′** instead of **4**. Correct identification of the metal atoms was considered; comparison of the M–O1 bond lengths and the residual indices associated with a model in which metal identities were switched favored the assignment illustrated in Figure 1. The non-H atoms of the cation were refined with anisotropic thermal parameters; isotropic thermal parameters were used for the carbon atoms of the tetraphenylborate anions. The phenyl rings of the BPh_4^- counterions were treated as rigid rings of idealized (C–C = 1.395 Å) geometry. Refinement of a model in which the carbon atoms of the tetraphenylborate anions were allowed independent positional parameters and anisotropic thermal parameters did not result in significantly better residual indices. Hydrogen atoms were included in calculated positions (C–H = 0.96 Å, $U_H = 1.2U_C$). Weighted ($w = [\sigma^2(R) + gF^2]^{-1}$) block-diagonal (maximum 103 parameters/cycle) least-squares refinement on F was taken to convergence (average shift/esd < 0.10 over the last 7 cycles). In the final ΔF map, the highest peak (1.21 e Å^{-3}) was located near O4; the minimum in the map was −0.9 e Å^{-3}. Analysis of

Table II. Fractional Atomic Coordinates ($\times 10^4$) and Isotropic Thermal Parameters ($\times 10^2$)[a] for **1'**

atom	x	y	z	B_{iso}	atom	x	y	z	B_{iso}
Fe2	953.5 (4)	3454.0 (4)	7407.1 (2)	189 (1)	C2F	2925 (3)	5956 (3)	4641 (2)	212 (8)
Fe3	2669.8 (4)	810.4 (4)	7961.9 (2)	167 (1)	C3F	2037 (3)	7020 (3)	4737 (2)	253 (8)
O1	1682 (2)	1701 (2)	7396 (1)	178 (5)	C4F	941 (3)	7156 (3)	4890 (2)	250 (9)
O2	537 (3)	3494 (2)	8225 (1)	299 (7)	C5F	728 (3)	6230 (3)	4945 (1)	229 (8)
O3	2624 (2)	3273 (2)	7404 (1)	299 (6)	C6F	1624 (3)	5175 (3)	4846 (1)	187 (7)
O4	3605 (2)	1582 (2)	7886 (1)	233 (6)	C1G	3322 (3)	2913 (3)	4496 (2)	190 (7)
O5	1537 (2)	1646 (2)	8547 (1)	254 (6)	C2G	3342 (3)	1936 (3)	4839 (2)	222 (8)
N1	1088 (2)	3661 (2)	6512 (1)	170 (6)	C3G	2867 (3)	1301 (3)	4722 (2)	268 (9)
N2	−623 (2)	3482 (2)	7295 (1)	206 (7)	C4G	2337 (3)	1628 (3)	4259 (2)	280 (9)
N3	475 (3)	5232 (2)	7180 (1)	219 (7)	C5G	2288 (3)	2593 (3)	3911 (2)	287 (9)
N4	2072 (2)	−468 (2)	8048 (1)	185 (6)	C6G	2768 (3)	3208 (3)	4032 (2)	243 (8)
N5	3787 (2)	−200 (2)	7333 (1)	174 (6)	C1H	4448 (3)	3193 (3)	5187 (1)	173 (7)
N6	3491 (2)	−436 (2)	8614 (1)	190 (6)	C2H	4176 (3)	3818 (3)	5612 (1)	185 (7)
C1	1434 (3)	1271 (3)	7028 (1)	182 (7)	C3H	4726 (3)	3382 (3)	6079 (2)	226 (8)
C2	1548 (3)	1669 (3)	6472 (1)	189 (8)	C4H	5596 (3)	2276 (3)	6137 (2)	261 (8)
C3	1318 (3)	1195 (3)	6108 (2)	222 (8)	C5H	5900 (3)	1631 (3)	5722 (2)	260 (9)
C4	981 (3)	333 (3)	6283 (2)	246 (8)	C6H	5340 (3)	2078 (3)	5261 (2)	229 (8)
C5	854 (3)	−25 (3)	6843 (2)	233 (8)	C1I	4773 (3)	3852 (2)	4102 (1)	171 (7)
C6	1071 (3)	430 (3)	7218 (2)	195 (8)	C2I	5933 (3)	3417 (3)	4137 (2)	225 (8)
C7	1914 (3)	2598 (3)	6279 (1)	188 (8)	C3I	6705 (3)	3534 (3)	3698 (2)	291 (9)
C8	−62 (3)	4077 (3)	6354 (1)	183 (8)	C4I	6346 (3)	4110 (3)	3198 (2)	284 (9)
C9	−768 (3)	3608 (3)	6768 (1)	192 (8)	C5I	5206 (3)	4567 (3)	3143 (2)	264 (9)
C10	−1534 (3)	3355 (3)	6616 (2)	227 (8)	C6I	4446 (3)	4443 (3)	3518 (2)	213 (8)
C11	−2198 (3)	2973 (3)	7018 (2)	310 (10)	B2	1576 (3)	1066 (3)	1073 (2)	212 (9)
C12	−2048 (3)	2834 (3)	7560 (2)	300 (10)	C1J	2090 (3)	785 (3)	1655 (1)	201 (8)
C13	−1255 (3)	3092 (3)	7681 (2)	250 (9)	C2J	2836 (3)	1163 (3)	1742 (2)	232 (8)
C14	1481 (3)	4551 (3)	6327 (1)	190 (8)	C3J	3261 (3)	905 (3)	2239 (2)	257 (8)
C15	782 (3)	5525 (3)	6651 (1)	183 (7)	C4J	2944 (3)	268 (3)	2677 (2)	253 (9)
C16	477 (3)	6642 (3)	6422 (1)	199 (7)	C5J	2206 (3)	−123 (3)	2615 (2)	249 (9)
C17	−177 (3)	7490 (3)	6748 (2)	227 (8)	C6J	1803 (3)	126 (3)	2112 (2)	209 (8)
C18	−494 (3)	7191 (3)	7294 (2)	219 (8)	C1K	1717 (3)	−138 (3)	933 (2)	235 (8)
C19	−141 (3)	6058 (3)	7496 (2)	246 (9)	C2K	2685 (4)	−1160 (3)	1050 (2)	320 (10)
C20	967 (3)	28 (3)	7821 (2)	202 (8)	C3K	2835 (5)	−2206 (4)	946 (2)	420 (10)
C21	2945 (3)	−1443 (3)	7764 (1)	199 (8)	C4K	2011 (4)	−2243 (3)	713 (2)	430 (10)
C22	4372 (3)	178 (3)	6912 (2)	200 (8)	C5K	1059 (4)	−1240 (4)	581 (2)	400 (10)
C23	4746 (3)	−252 (3)	6421 (2)	255 (9)	C6K	936 (3)	−225 (3)	688 (2)	309 (9)
C24	4521 (3)	−1114 (3)	6363 (2)	269 (9)	C1L	2253 (3)	1610 (3)	573 (1)	208 (8)
C25	3940 (3)	−1523 (3)	6793 (2)	240 (9)	C2L	3046 (3)	1029 (3)	157 (2)	234 (8)
C26	3579 (3)	−1044 (3)	7273 (1)	183 (8)	C3L	3579 (3)	1533 (3)	−259 (2)	277 (9)
C27	1920 (3)	−837 (3)	8646 (2)	226 (8)	C4L	3336 (3)	2657 (3)	−280 (2)	270 (9)
C28	2949 (3)	−1049 (3)	8884 (1)	208 (8)	C5L	2561 (3)	3261 (3)	125 (2)	276 (9)
C29	3302 (3)	−1788 (3)	9360 (2)	261 (9)	C6L	2039 (3)	2745 (3)	538 (2)	256 (9)
C30	4238 (3)	−1892 (3)	9551 (2)	280 (10)	C1M	227 (3)	2025 (3)	1118 (2)	225 (8)
C31	4807 (3)	−1284 (3)	9268 (2)	262 (9)	C2M	−319 (3)	2553 (3)	644 (2)	295 (9)
C32	4408 (3)	−553 (3)	8797 (1)	220 (8)	C3M	−1437 (3)	3398 (3)	651 (2)	340 (10)
C33	937 (3)	2706 (3)	8610 (2)	231 (8)	C4M	−2056 (4)	3780 (4)	1135 (2)	370 (10)
C34	678 (3)	2977 (3)	9180 (2)	288 (9)	C5M	−1551 (3)	3306 (3)	1614 (2)	310 (10)
C35	3454 (3)	2579 (3)	7648 (2)	253 (8)	C6M	−438 (3)	2442 (3)	1596 (2)	242 (8)
C36	4401 (4)	2883 (4)	7667 (2)	460 (10)	C1N	3682 (5)	3733 (5)	1890 (3)	570 (20)
C37	752 (4)	−190 (3)	5874 (2)	380 (10)	C2N	3311 (5)	3687 (5)	2485 (2)	590 (20)
C38	4281 (9)	3297 (9)	8165 (4)	470 (30)	C3N	2793 (5)	4249 (5)	1497 (2)	590 (20)
C38'	4955 (7)	2405 (8)	8137 (4)	530 (20)	O4N	4663 (4)	3372 (7)	1703 (2)	1370 (30)
C39	149 (5)	4226 (4)	9234 (2)	420 (10)	C1P	5225 (9)	4991 (8)	448 (6)	1530 (50)
B1	3835 (3)	3723 (3)	4623 (2)	158 (8)	C2P	5000	5000	0	4720 (70)
C1F	2751 (3)	4994 (3)	4694 (1)	169 (7)					

[a] Estimated standard deviations in the least significant digit are given in parentheses.

variance as a function of Bragg angle, intensity, reflection indices, etc., showed no significant trend.

Refinement of the model described above gave U_{iso} values for Fe and Zn (0.0162 and 0.0290, respectively) that suggest some degree of disorder involving the two metal centers. Calculations using variable site occupancy factors (sof) and the above assignments for Fe and Zn supported partial, but not random, disorder. These calculations resulted in a modest difference in the sof values for Fe (1.02) and Zn (0.91) and an insignificant reduction (0.002) in the R value. Since the calculations indicated that Fe and Zn predominate at the sites shown in Figure 1, the final structural model incorporated fixed site occupancy factors of 1.0 for these two atoms. While ignoring the small degree of disorder possibly present, this simple model has the advantage of eliminating reliance on simultaneous refinement of the highly correlated thermal and site occupancy parameters to judge the degree of such disorder.

The final fractional atomic coordinates for **4'** are contained in Table IV, while bond lengths and angles for the dinuclear complex cation are reported in Table V. A complete listing of bond lengths and angles, thermal parameters, hydrogen atom coordinates, and F_o/F_c tables has been supplied as supplementary material. The structure of the cation is shown in Figure 1b, together with the numbering scheme used.

Physical Methods. ^{1}H NMR spectra of the binuclear metal complexes were obtained on an IBM AF-300 NMR spectrometer. Samples were made in CD_3COCD_3 at concentrations ranging from 5 to 10 mM, which required 5000 scans to obtain adequate signal-to-noise ratios. Variable-temperature NMR experiments were performed on a Nicolet NT-300 NMR spectrometer; temperature calibration was accomplished with a methanol/HCl solution.[23a] EPR spectra were obtained at X-band with a Varian E-109 spectrometer equipped with an Oxford Instruments ESR-10 liquid helium cryostat. Samples were prepared under nitrogen, with all solvents distilled prior to use and degassed by five freeze–pump–thaw cycles. Mössbauer spectra were obtained in the laboratory of Prof. Eckard Münck.

Visible spectra of the complexes in acetonitrile were obtained by using Hewlett-Packard 8451A diode array and Cary 219 spectrophotometers. All samples were prepared under nitrogen. Near-IR spectra were re-

(23) (a) Van Geet, A. L. *Anal. Chem.* **1980**, *42*, 679–680. (b) Stankovich, M. T. *Anal. Biochem.* **1980**, *109*, 295–308.

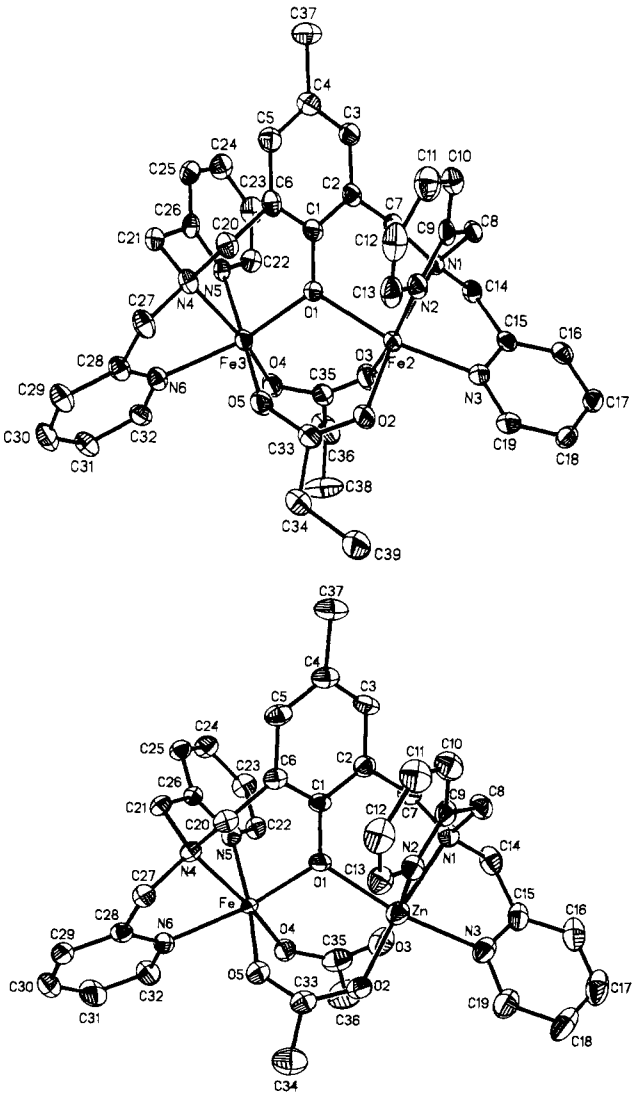

Figure 1. Plot of the structures of (a) $[Fe^{II}Fe^{III}BPMP(OPr)_2]^{2+}$ and (b) $[Zn^{II}Fe^{III}BPMP(OAc)_2]^{2+}$, showing 50% probability ellipsoids. The hydrogen atoms are omitted for clarity.

corded with a Cary 14 spectrophotometer interfaced to a OLIS computer system. All samples were prepared in CD_3CN under nitrogen. The bands in the near-IR spectra were fit to obtain E_{OP} and $\Delta\nu_{1/2}$ using a program developed by Dr. C. Loudon. The program fit the data to a normal curve by regressing ln A versus $(E - E_{OP})^2$, where A is the absorbance, E is the wavenumber, and E_{OP} is the value of E when A is at its maximum. Because sampling rate decreases with increasing wavenumber, it was necessary to subsample the data at regular intervals to eliminate the skewed distribution. E_{OP} can then be estimated as the mean of the subsampled data, weighting each wavenumber by its corresponding absorbance value. The value of $\Delta\nu_{1/2}$ was determined from the slope of the regression line (m) as $\Delta\nu_{1/2} = 1.67\ (-m)^{-1/2}$. Examination of residuals gave no evidence for the presence of more than one peak.

Resonance Raman spectra were obtained on CD_3CN solutions of the complexes using a Spex 1403 spectrometer interfaced to a Spex Datamate with the lines of a Spectra Physics 375B dye laser (Rhodamine 6G) pumped by a Spectra Physics 171 argon ion laser. Spectra were recorded at room temperature with a spinning quartz cell with the incident laser beam 90° relative to the scattered light collected. Raman frequencies are referenced against the 1102-cm^{-1} peak of CD_3CN.

Electrochemical studies were performed with a BAS 100 electrochemical analyzer (Bioanalytical Systems, Inc., West Lafayette, IN). All experiments were done under nitrogen at ambient temperature in solutions of acetonitrile with 0.1 M tetrabutylammonium tetrafluoroborate as the supporting electrolyte. The acetonitrile was distilled under nitrogen from CaH_2 just prior to use. Cyclic voltammograms (CV) were obtained by using a three-component system consisting of a platinum disk working electrode, a platinum wire auxiliary electrode, and a BAS saturated calomel reference electrode containing a Vycor plug to separate it from the bulk solution. IR compensation was achieved before each was recorded. The ferrocinium/ferrocene couple was used to monitor reference electrode and was observed at +422 mV. Controlled potential coulometry (CPC) was performed by using a spectroelectrochemical cell designed by Prof. M. Stankovich.[23b] The cell consists of an anaerobic cuvette which is fitted with a small Teflon stirbar, a coiled gold wire working electrode, a silver–silver chloride auxiliary electrode, and a silver–silver chloride reference electrode. Vycor plugs were used at all liquid junctions. CPC experiments were performed under nitrogen in a Hewlett-Packard 8451A diode array spectrophotometer.

Table III. Selected Bond Lengths (Å) and Angles (deg) for **1′**[a]

	a. Bond Lengths		
Fe2–O1	2.090 (2)	Fe3–O1	1.943 (2)
Fe2–O2	2.029 (2)	Fe3–O5	1.983 (2)
Fe2–O3	2.145 (3)	Fe3–O4	1.945 (2)
Fe2–N1	2.195 (3)	Fe3–N4	2.185 (3)
Fe2–N2	2.186 (3)	Fe3–N5	2.155 (3)
Fe2–N3	2.141 (3)	Fe3–N6	2.128 (3)
O1–C1	1.366 (4)	O2–C33	1.258 (4)
O3–C35	1.242 (4)	O4–C35	1.284 (4)
O5–C33	1.293 (4)	N1–C7	1.490 (4)
N2–C9	1.347 (4)	N1–C8	1.486 (4)
N2–C13	1.344 (5)	N1–C14	1.486 (4)
N3–C15	1.343 (4)	N3–C19	1.342 (4)
N4–C20	1.495 (4)	N5–C26	1.343 (4)
N4–C21	1.489 (4)	N5–C22	1.345 (4)
N4–C27	1.485 (4)	N6–C28	1.344 (4)
N6–C32	1.338 (4)	C1–C2	1.393 (5)
C1–C6	1.399 (5)	C3–C4	1.398 (5)
C2–C3	1.386 (5)	C4–C5	1.393 (5)
C2–C7	1.510 (5)	C4–C37	1.524 (5)
C5–C6	1.382 (5)	C6–C20	1.500 (5)
C8–C9	1.505 (5)	C9–C10	1.378 (5)
C10–C11	1.389 (5)	C11–C12	1.385 (6)
C12–C13	1.380 (6)	C14–C15	1.503 (5)
C15–C16	1.379 (5)	C16–C17	1.384 (5)
C17–C18	1.385 (5)	C18–C19	1.375 (5)
C21–C26	1.502 (5)	C22–C23	1.380 (5)
C23–C24	1.380 (5)	C24–C25	1.375 (5)
C25–C26	1.387 (5)	C27–C28	1.502 (5)
C28–C29	1.387 (5)	C29–C30	1.379 (5)
C30–C31	1.374 (5)	C31–C32	1.387 (5)
C33–C34	1.493 (5)	C35–C36	1.529 (6)
C36–C38	1.44 (1)	C36–C38′	1.40 (1)
C34–C39	1.511 (6)	Fe2–Fe3	3.365 (1)
	b. Bond Angles		
O3–Fe2–O2	94.0 (1)	O3–Fe2–O1	88.47 (9)
O3–Fe2–N1	93.8 (1)	O3–Fe2–N2	170.5 (1)
O3–Fe2–N3	85.2 (1)	O2–Fe2–O1	99.93 (9)
O2–Fe2–N1	169.5 (1)	O2–Fe2–N2	94.2 (1)
O2–Fe2–N3	96.3 (1)	O1–Fe2–N1	87.22 (9)
O1–Fe2–N2	85.5 (1)	O1–Fe2–N3	163.0 (1)
N1–Fe2–N2	78.6 (1)	N1–Fe2–N3	77.5 (1)
N2–Fe2–N3	98.5 (1)	O4–Fe3–O5	95.5 (1)
O4–Fe3–O1	102.1 (1)	O4–Fe3–N4	164.3 (1)
O4–Fe3–N5	91.1 (1)	O4–Fe3–N6	94.1 (1)
O5–Fe3–O1	93.5 (1)	O5–Fe3–N4	95.3 (1)
O5–Fe3–N5	173.4 (1)	O5–Fe3–N6	85.3 (1)
O1–Fe3–N4	88.6 (1)	O1–Fe3–N5	85.1 (1)
O1–Fe3–N6	163.8 (1)	N4–Fe3–N5	78.3 (1)
N4–Fe3–N6	75.4 (1)	N5–Fe3–N6	94.2 (1)
Fe2–O1–Fe3	113.1 (1)	Fe2–O1–C1	121.3 (2)
Fe2–O2–C33	128.6 (2)	Fe2–O3–C35	134.4 (3)
Fe2–N1–C7	113.2 (2)	Fe2–N2–C13	125.1 (2)
Fe2–N1–C8	108.5 (2)	Fe2–N1–C14	103.6 (2)
Fe2–N3–C15	114.1 (2)	Fe2–N3–C19	127.2 (2)
Fe2–N2–C9	114.2 (2)	Fe3–O1–C1	125.6 (2)
Fe3–O4–C35	130.7 (2)	Fe3–O5–C33	135.0 (2)
Fe3–N4–C20	111.0 (2)	Fe3–N4–C21	109.6 (2)
Fe3–N4–C27	105.2 (2)	Fe3–N5–C22	122.9 (2)
Fe3–N5–C26	115.1 (2)	Fe3–N6–C28	115.0 (2)
Fe3–N6–C32	124.8 (2)		

[a] Estimated standard deviations in the least significant digit are in parentheses.

Results and Discussion

Synthesis. Several of the binuclear iron–oxo proteins have accessible $Fe^{II}Fe^{III}$ oxidation states, the properties of which are

Table IV. Fractional Atomic Coordinates ($\times 10^4$) and Isotropic Thermal Parameters ($Å^2 \times 10^3$)[a] for **4'**

atom	x	y	z	U_{iso}[b]	atom	x	y	z	U_{iso}[b]
Fe	4606 (1)	4549 (1)	7796 (1)	16 (1)*	C38	7314 (2)	3950 (2)	5444 (1)	22 (1)
Zn	3835 (1)	2580 (1)	8326 (1)	29 (1)*	C39	8379 (2)	4557 (2)	5766 (1)	28 (1)
O1	3698 (2)	3234 (2)	7528 (1)	24 (1)*	C40	8505 (2)	5528 (2)	5950 (1)	29 (1)
O2	5483 (2)	3079 (2)	8814 (1)	32 (1)*	C41	7566 (2)	5891 (2)	5813 (1)	27 (1)
O3	3472 (3)	3739 (2)	8879 (2)	40 (1)*	C42	6500 (2)	5284 (2)	5491 (1)	27 (1)
O4	4281 (3)	5058 (2)	8631 (1)	32 (1)*	C43	6374 (2)	4313 (2)	5307 (1)	23 (1)
O5	6017 (2)	4181 (2)	8310 (2)	33 (1)*	C44	5875 (2)	2178 (2)	4728 (1)	23 (1)
N1	2088 (3)	1798 (2)	7802 (2)	26 (1)*	C45	5348 (2)	1425 (2)	4915 (1)	24 (1)
N2	4028 (3)	1401 (2)	7636 (2)	25 (1)*	C46	4263 (2)	912 (2)	4503 (1)	32 (1)
N3	3517 (3)	1920 (2)	9079 (2)	33 (1)*	C47	3704 (2)	1151 (2)	3903 (1)	35 (1)
N4	4976 (3)	4248 (2)	6818 (2)	20 (1)*	C48	4232 (2)	1904 (2)	3717 (1)	35 (1)
N5	3251 (3)	4886 (2)	7114 (2)	23 (1)*	C49	5317 (2)	2418 (2)	4129 (1)	29 (1)
N6	5755 (3)	5825 (2)	7878 (2)	24 (1)*	C50	8076 (2)	2620 (2)	4721 (1)	21 (1)
C1	3092 (3)	2731 (3)	6854 (2)	22 (1)*	C51	9222 (2)	2830 (2)	5081 (1)	29 (1)
C2	1986 (3)	2233 (3)	6705 (2)	26 (1)*	C52	9963 (2)	2749 (2)	4711 (1)	31 (1)
C3	1394 (3)	1677 (3)	6021 (2)	28 (1)*	C53	9557 (2)	2457 (2)	3981 (1)	30 (1)
C4	1875 (4)	1601 (3)	5502 (2)	29 (2)*	C54	8411 (2)	2247 (2)	3622 (1)	32 (1)
C5	2967 (4)	2127 (3)	5671 (2)	28 (2)*	C55	7671 (2)	2328 (2)	3992 (1)	27 (1)
C6	3585 (3)	2694 (3)	6341 (2)	22 (1)*	C56	7654 (2)	2388 (2)	5912 (1)	20 (1)
C7	1497 (3)	2253 (3)	7283 (2)	28 (2)*	C57	8003 (2)	1556 (2)	5855 (1)	25 (1)
C8	2068 (4)	821 (3)	7458 (2)	31 (2)*	C58	8296 (2)	1196 (2)	6434 (1)	27 (1)
C9	3066 (4)	778 (3)	7229 (2)	28 (2)*	C59	8241 (2)	1670 (2)	7070 (1)	28 (1)
C10	3016 (4)	98 (3)	6647 (2)	37 (2)*	C60	7892 (2)	2503 (2)	7128 (1)	32 (1)
C11	3972 (4)	58 (3)	6493 (3)	38 (2)*	C61	7599 (2)	2862 (2)	6549 (1)	26 (1)
C12	4966 (4)	696 (3)	6914 (2)	37 (2)*	C62	−502 (2)	1422 (2)	1431 (1)	26 (1)
C13	4963 (4)	1355 (3)	7481 (2)	30 (2)*	C63	12 (2)	947 (2)	1014 (1)	30 (1)
C14	1614 (4)	1808 (3)	8367 (2)	35 (2)*	C64	760 (2)	444 (2)	1292 (1)	35 (1)
C15	2423 (4)	1635 (3)	8992 (3)	33 (2)*	C65	994 (2)	415 (2)	1987 (1)	36 (1)
C16	2056 (5)	1210 (3)	9450 (2)	44 (2)*	C66	480 (2)	890 (2)	2404 (1)	37 (1)
C17	2837 (5)	1080 (3)	10007 (3)	52 (2)*	C67	−268 (2)	1393 (2)	2126 (1)	34 (1)
C18	3963 (5)	1372 (3)	10100 (2)	52 (2)*	C68	−1875 (2)	1714 (2)	233 (1)	28 (1)
C19	4273 (5)	1799 (3)	9624 (2)	41 (2)*	C69	−1118 (2)	2001 (2)	−93 (1)	32 (1)
C20	4781 (3)	3219 (3)	6525 (2)	24 (1)*	C70	−1435 (2)	1737 (2)	−821 (1)	38 (1)
C21	4291 (3)	4664 (3)	6305 (2)	22 (1)*	C71	−2507 (2)	1185 (2)	−1223 (1)	41 (1)
C22	2367 (3)	5088 (3)	7270 (2)	26 (2)*	C72	−3264 (2)	897 (2)	−898 (1)	44 (1)
C23	1502 (4)	5279 (3)	6809 (2)	32 (2)*	C73	−2948 (2)	1162 (2)	−170 (1)	33 (1)
C24	1535 (4)	5268 (3)	6143 (2)	32 (2)*	C74	−833 (2)	3198 (2)	1401 (1)	28 (1)
C25	2417 (3)	5042 (3)	5968 (2)	26 (1)*	C75	71 (2)	3597 (2)	2022 (1)	29 (1)
C26	3271 (3)	4854 (3)	6463 (2)	20 (1)*	C76	496 (2)	4571 (2)	2256 (1)	36 (1)
C27	6167 (3)	4728 (3)	7025 (2)	24 (1)*	C77	18 (2)	5147 (2)	1871 (1)	44 (1)
C28	6384 (3)	5718 (3)	7460 (2)	23 (1)*	C78	−886 (2)	4748 (2)	1250 (1)	49 (1)
C29	7157 (3)	6462 (3)	7445 (2)	28 (2)*	C79	−1311 (2)	3774 (2)	1016 (1)	40 (1)
C30	7315 (4)	7343 (3)	7869 (2)	35 (2)*	C80	−2491 (2)	1806 (1)	1431 (2)	26 (1)
C31	6664 (4)	7452 (3)	8286 (3)	42 (2)*	C81	−2850 (2)	2531 (1)	1768 (2)	34 (1)
C32	5901 (4)	6683 (3)	8284 (2)	35 (2)*	C82	−3685 (2)	2323 (1)	2057 (2)	42 (1)
C33	6216 (3)	3648 (3)	8705 (2)	26 (2)*	C83	−4159 (2)	1390 (1)	2008 (2)	41 (1)
C34	7421 (4)	3698 (4)	9076 (3)	41 (2)*	C84	−3800 (2)	665 (1)	1670 (2)	39 (1)
C35	3848 (4)	4624 (4)	9001 (2)	39 (2)*	C85	−2966 (2)	873 (1)	1381 (2)	34 (1)
C36	3744 (5)	5263 (4)	9627 (3)	58 (3)*	C90	1532 (5)	3901 (5)	858 (3)	72 (3)*
C37	1247 (4)	941 (3)	4787 (2)	40 (2)*	C91	1366 (7)	3633 (5)	126 (4)	81 (4)*
B1	7219 (4)	2779 (3)	5197 (2)	20 (2)	N90	1214 (9)	3407 (5)	−471 (4)	102 (5)*
B2	−1430 (4)	2032 (3)	1116 (2)	23 (2)					

[a] Estimated standard deviations in the least significant digit are given in parentheses. [b] For values with asterisks, the equivalent isotropic U is defined as one-third of the trace of the U tensor.

not fully understood.[1,2,4,5] Using the synthetic model approach to examine more thoroughly the structure and properties of diiron(II,III) centers, we have synthesized a series of triply bridged binuclear metal complexes of the ligand HBPMP. The synthesis of the $Fe^{II}Fe^{III}$ complexes was initially achieved by treating a methanolic solution of HBPMP with 2 equiv of $Fe(NO_3)_3 \cdot 9H_2O$ and 3 equiv of sodium propionate (or sodium benzoate), followed by metathesis with either $NaBPh_4$ or NH_4PF_6. The only metal species isolated were the mixed valence diiron complexes, which indicated the participation of a redox process during complex formation. It appeared that reduction occurred after the triply bridged unit was formed because of the pronounced color change observed when the carboxylates were added to the reaction mixture. Electrochemical studies of these complexes show that the diiron(III,III) species are strong oxidants (vide infra), suggesting that the reductant may be the methanol solvent.

Interestingly, when a methanolic solution of HBPMP was treated with only 1 equiv of Fe^{III}, the predominant species generated was a mononuclear Fe^{III} complex. Present in this mononuclear Fe^{III} species is a vacant site which is poised to bind other metal ions. When treated with divalent metal ions (e.g., Fe^{II} and Zn^{II}) and the appropriate carboxylate salt, this ferric species afforded the corresponding triply bridged $Fe^{II}Fe^{III}$ and $Zn^{II}Fe^{III}$ complexes. The $Fe^{II}Fe^{III}$ complexes obtained by this method have the same properties as the complexes generated by method A. When the monoferric species was treated with the trivalent metal ion Ga^{III}, a redox reaction occurred, similar to that observed when 2 equiv of Fe^{III} was used, to yield the yellow $Fe^{II}Ga^{III}$ complex. Other products were observed in this reaction, which were removed by chromatography, suggesting that the redox process was not as efficient as when only ferric ions were involved.

Description of Solid-State Structures. Complex 1'. The structure of **1'** confirms the mixed valence nature of this binuclear complex by exhibiting discrete iron(II) and iron(III) centers. The metal centers of this complex cation are bridged by the phenolate oxygen atom of $BPMP^-$ and by two propionate ligands, thus giving what increasingly appears to be a thermodynamically favored core structure. Examples of structurally characterized diiron complexes with similar triply bridged cores include hemerythrin model complexes[7,15,24,25] and $[Fe_2HXTA(OAc)_2]^-$ (**6**),[26] as well as

Table V. Selected Bond Lengths (Å) and Angles (deg) for **4′**[a]

	a. Bond Lengths		
Fe–O1	1.982 (3)	Zn–O1	2.067 (3)
Fe–O4	1.939 (3)	Zn–O2	1.999 (3)
Fe–O5	2.055 (3)	Zn–O3	2.086 (3)
Fe–N4	2.193 (4)	Zn–N1	2.184 (3)
Fe–N5	2.118 (3)	Zn–N2	2.138 (3)
Fe–N6	2.146 (3)	Zn–N3	2.106 (4)
O1–C1	1.366 (4)	O2–C33	1.261 (6)
O3–C35	1.275 (6)	O4–C35	1.283 (6)
O5–C33	1.262 (6)	N1–C7	1.486 (6)
N1–C8	1.486 (5)	N1–C14	1.469 (7)
N2–C9	1.339 (4)	N2–C13	1.346 (7)
N3–C15	1.350 (7)	N3–C19	1.330 (6)
N4–C20	1.486 (5)	N4–C21	1.490 (5)
N4–C27	1.473 (5)	N5–C22	1.341 (6)
N5–C26	1.349 (5)	N6–C28	1.355 (6)
N6–C32	1.336 (5)	C1–C2	1.403 (6)
C1–C6	1.387 (6)	C2–C3	1.399 (5)
C2–C7	1.506 (7)	C3–C4	1.386 (7)
C4–C5	1.394 (6)	C4–C37	1.504 (5)
C5–C6	1.389 (5)	C6–C20	1.503 (5)
C8–C9	1.505 (7)	C9–C10	1.390 (6)
C10–C11	1.370 (8)	C11–C12	1.379 (6)
C12–C13	1.375 (7)	C14–C15	1.512 (6)
C15–C16	1.389 (8)	C16–C17	1.369 (7)
C17–C18	1.387 (9)	C18–C19	1.392 (8)
C21–C26	1.507 (6)	C22–C23	1.359 (6)
C23–C24	1.391 (7)	C24–C25	1.369 (7)
C25–C26	1.386 (6)	C27–C28	1.504 (5)
C28–C29	1.372 (6)	C29–C30	1.375 (6)
C30–C31	1.376 (8)	C31–C32	1.376 (7)
C33–C34	1.504 (6)	C35–C36	1.504 (8)
	b. Bond Angles		
O1–Fe–O4	99.9 (1)	O1–Zn–O3	87.2 (1)
O4–Fe–O5	95.5 (1)	O1–Zn–N1	88.9 (1)
O4–Fe–N4	168.7 (1)	O3–Zn–N1	94.7 (1)
O1–Fe–N5	89.1 (1)	O2–Zn–N2	92.9 (1)
O5–Fe–N5	170.0 (1)	N1–Zn–N2	79.8 (1)
O1–Fe–N6	165.1 (1)	O2–Zn–N3	96.5 (1)
O5–Fe–N6	84.6 (1)	N1–Zn–N3	78.0 (1)
N5–Fe–N6	92.4 (1)	O1–Zn–O2	97.6 (1)
O1–Fe–O5	91.5 (1)	O2–Zn–O3	93.1 (1)
O1–Fe–N4	89.3 (1)	O2–Zn–N1	170.1 (1)
O5–Fe–N4	90.7 (1)	O1–Zn–N2	87.1 (1)
O4–Fe–N5	94.3 (1)	O3–Zn–N2	172.1 (1)
N4–Fe–N5	79.2 (1)	O1–Zn–N3	164.5 (1)
O4–Fe–N6	94.7 (1)	O3–Zn–N3	85.6 (1)
N4–Fe–N6	76.4 (1)	N2–Zn–N3	98.7 (1)
Fe–O1–Zn	116.1 (1)	Zn–O1–C1	119.7 (2)
Fe–O1–C1	123.8 (3)	Zn–O2–C33	132.3 (3)
Fe–O4–C35	129.3 (3)	Zn–O3–C35	132.7 (4)
Fe–O5–C33	134.5 (3)	Zn–N1–C7	110.9 (2)
Fe–N4–C20	111.0 (3)	Zn–N1–C8	107.9 (3)
Fe–N4–C21	110.0 (3)	Zn–N1–C14	104.9 (2)
Fe–N4–C27	104.0 (2)	Zn–N2–C9	114.3 (3)
Fe–N5–C22	125.3 (3)	Zn–N2–C13	125.1 (2)
Fe–N5–C26	116.5 (3)	Zn–N3–C15	114.1 (3)
Fe–N6–C28	114.2 (2)	Zn–N3–C19	126.8 (4)
Fe–N6–C32	127.4 (3)		

[a] Estimated standard deviations in the least significant digit are given in parentheses.

methemerythrin azide.[6] In a variation on this theme, we have recently reported the structure of a doubly bridged (μ-oxo)(μ-benzoato)diiron(III) compound.[27] In all of these previous cases, the metal–metal separation is constrained by the carboxylate bridge(s) to be less than 3.5 Å. The Fe–Fe distance in **1′** of 3.365 (1) Å is comparable to the metal–metal separations in **6** and in $[(HBpz_3Fe)_2OH(OAc)_2]^+$[24] (3.442 and 3.439 (1) Å, respectively), which have phenolato or hydroxo ligands as the bridging groups. The Fe2–O1–Fe3 angle is 113.1 (1)°, and the phenyl ring of the $BPMP^-$ ligand is twisted relative to the Fe2–O1–Fe3 plane. The resulting dihedral angle between the plane defined by the C1–C6 carbon atoms of the phenolate ring and the Fe2–O1–Fe3 plane is 51.3°. This twist of the phenolate ring from the Fe–O–Fe plane has also been observed in **6**, in which a dihedral angle of 40° was observed.[26]

Complex **1′** does not exhibit any crystallographically imposed symmetry, resulting, remarkably, in the observation of distinct ferrous and ferric sites in the complex cation. The unique iron centers are manifested in the significant differences found for the Fe–O bond lengths of the two iron centers. The length of the Fe2–O1 bond, 2.090 (2) Å, compares favorably with those found for the Fe^{II}–O(phenolate) bonds (2.062 (1) and 2.052 (1) Å) in $[Fe_2BPMP(OPr)_2]^+$,[18] while that for the Fe3–O1 bond, 1.943 (2) Å, is in the range of other Fe^{III}–O(phenolate) bonds found in complexes such as $[Fe_2(HDP)_2O(OBz)]^+$ (1.924 (6) and 1.931 (6) Å)[27] and **4′** (1.982 (3) Å). The average Fe^{III}–O values of 1.96 Å and Fe^{II}–O values of 2.09 Å found for **1′** compare with the average Fe^{III}–O bond lengths found in $[(HBpz_3Fe)_2OH(OAc)_2]^+$ (1.97 Å)[24] and the average Fe^{II}–O bond lengths observed for $[Fe_2(OH)(OAc)_2(Me_3TACN)_2]^+$[15,25] and $[Cr^{III}Fe^{II}(OH)(OAc)_2(Me_3TACN)_2]^{2+}$[28] of 2.08 and 2.06 Å, respectively.

The asymmetry found about the metal ions in **1′** has been observed in other mixed valence metal complexes. For example, X-ray and Mössbauer analyses of mixed valence dialkyl- and dihalobiferrocenium salts reveal that several of these complexes contain valence-trapped Fe^{II} and Fe^{III} centers.[29] Hendrickson has attributed the localized valence sites to the influence of the solid-state environment around the mixed valence cation. Comparable asymmetry about the Mn^{II} and Mn^{III} atoms in $[Mn^{II}Mn^{III}BPMP(O_2CR)_2]^{2+}$ complexes (R = C_6H_5,[30a] CH_3[30b]) has also been taken to indicate valence trapping in the solid state. While the present results do not allow us to determine the exact causes for the valence-trapped Fe^{II} and Fe^{III} sites in the solid state for **1′**, the Mössbauer results for **1** indicate that only in the crystalline solid is the extra electron trapped at the Fe2 site (vide infra), suggesting that the solid-state environment contributes to the localized valency found in **1**.

In the binuclear cation of **1′**, each of the iron centers has a tertiary amino nitrogen atom and one of the pyridyl groups trans to oxygen atoms of the propionate bridges. The shorter Fe3–O4(propionate) (1.945 (2) Å) and Fe2–O2(propionate) (2.029 (2) Å) bonds are exhibited by the propionate oxygen atoms that are trans to the tertiary amino nitrogen atoms (N4 and N1, respectively). Examination of the roughly octahedral coordination array about Fe^{III} reveals that one Fe^{III}–N bond is significantly longer than the others (Fe3–N4 = 2.185 (3) Å, Fe3–N5 = 2.155 (3) Å, Fe3–N6 = 2.128 (3) Å). Equally long Fe–N bonds have been reported in hemerythrin model compounds,[7,24] but the unusual lengths of those bonds have been ascribed to the structural trans effect of a μ-oxo bridge.[7a] This clearly cannot be a factor in lengthening Fe3–N4 in **1′**. Furthermore, the N1–Fe2–N2, N1–Fe2–N3, N4–Fe3–N5, and N4–Fe3–N6 angles in **1′** are significantly less than 90° (78.6 (1)°, 77.5 (1)°, 78.3 (1)°, and 75.4 (1)°, respectively). Given the nature of $BPMP^-$, the structural results suggest that constraints associated with the short, one-carbon "arm lengths" from the phenolato ring and pyridyl rings to the tertiary amino nitrogen atom give rise to the long Fe2–N1 and Fe3–N4 bond lengths.

(24) Armstrong, W. H.; Lippard, S. J. *J. Am. Chem. Soc.* **1984**, *106*, 4632–4633.
(25) Chaudhuri, P.; Wieghardt, K.; Nuber, B.; Weiss, J. *Angew. Chem., Intl. Ed. Engl.* **1985**, *24*, 778–779.
(26) (a) Murch, B. P. Ph.D. Thesis, Cornell University, Ithaca, NY, 1987. (b) Murch, B. P.; Bradley, F. C.; Que, L., Jr. *J. Am. Chem. Soc.* **1986**, *108*, 5027–5028.
(27) Yan, S.; Que, L., Jr.; Taylor, L. F.; Anderson, O. P. *J. Am. Chem. Soc.* **1988**, *110*, 5222–5224.
(28) Chaudhuri, P.; Winter, M.; Küppers, H.; Wieghardt, K.; Nuber, B.; Weiss, J. *Inorg. Chem.* **1987**, *26*, 3302–3310.
(29) (a) Dong, T.-Y.; Hendrickson, D. H.; Iwai, K.; Cohn, M. J.; Geib, S. J.; Rheingold, A. L.; Sano, H.; Motoyama, I.; Nakashima, S. *J. Am. Chem. Soc.* **1985**, *107*, 7996–8008. (b) Dong, T.-Y.; Hendrickson, D. H.; Pierpont, C. G.; Moore, M. F. *J. Am. Chem. Soc.* **1986**, *108*, 963–971.
(30) (a) Suzuki, M.; Mikuriya, M.; Murata, S.; Uehara, A.; Oshio, H.; Kida, S.; Saito, K. *Bull. Chem. Soc. Jpn.* **1987**, *60*, 4305–4312. (b) Diril, H.; Chang, H.-R.; Zhang, X.; Larsen, S. R.; Potenza, J. A.; Pierpont, C. G.; Schugar, H. J.; Isied, S. S.; Hendrickson, D. N. *J. Am. Chem. Soc.* **1987**, *109*, 6207–6208.

The structure observed for **1'** allows us to gain some insights into the geometry about the $Fe^{II}Fe^{III}$ centers in Hr. EXAFS measurements found that the Fe–Fe distance in semimethemerythrin azide is 3.44 Å,[10] which is significantly longer than the Fe–Fe distance in methemerythrin azide (3.25 Å[5] and 3.20 Å,[31] as determined by X-ray analysis and EXAFS, respectively). The longer Fe–Fe separation in semimethemerythrin azide has been attributed to the protonation of the μ-oxo bridge present in methemerythrin azide, resulting in a μ-hydroxo moiety in the semimethemerythrin form.[1,10,32] The Fe–Fe distance of 3.365 Å found for **1'** compares favorably with that found in semimethemerythrin azide and supports the suggestion that the diiron center in semimethemerythrin contains a μ-hydroxo bridge. We expect that the μ-phenoxo bridge present in **1'** should be much better at approximating the geometric characteristics of a μ-hydroxo than a μ-oxo bridging moiety. Of course, structural characterization of additional diiron(II,III) complexes is necessary before we can gain a complete understanding of the factors that influence the geometry of triply bridged $Fe^{II}Fe^{III}$ centers.

Complex 4'. The heterobimetallic Fe/Zn and Fe/Ga complexes were synthesized as models for diiron(II,III) complexes. These complexes allowed us to investigate the physical properties of individual Fe^{II} and Fe^{III} centers in the same structural environment as our $Fe^{II}Fe^{III}$ complexes. It is thus necessary to ensure that these heterobimetallic complexes have the same general triply bridged structure that was found for **1'**.

The structure of **4'** demonstrates that this is so for the Fe/Zn species. As was the case for **1'**, the metal centers of this discrete, heterobinuclear cation are bridged by the phenolate oxygen atom of $BPMP^-$ and by two carboxylate (acetate) ligands. Furthermore, this complex exhibits the same coordination preferences as **1'**. Each of the metal centers has a tertiary amino nitrogen atom and a pyridyl group trans to the oxygen atoms of the acetate bridges. The shorter Fe–O4(acetate) (1.939 (3) Å) and Zn–O2(acetate) (1.999 (3) Å) bonds are exhibited by the acetate oxygen atoms that are trans to the tertiary amino nitrogen atoms (N4 and N1, respectively). Examination of the roughly octahedral coordination array about Fe revealed that one Fe–N bond was significantly longer than the others (Fe–N4 = 2.193 (4) Å, cf. Fe–N5 = 2.118 (3) Å and Fe–N6 = 2.146 (3) Å). Also, the N4–Fe–N5 and N4–Fe–N6 angles in **4'** are significantly less than 90° (79.2 (1)° and 76.4 (1)°, respectively). These structural preferences are consistent with those observed for **1'** and suggest that the nature of $BPMP^-$ gives rise to these distorted metric parameters.

The ionic radii for six-coordinate Zn^{II} (0.88 Å) and high-spin, six-coordinate Fe^{III} (0.78 Å) differ significantly,[33] and the Fe–O1 (1.982 (3) Å) and Zn–O1 (2.067 (3) Å) bond lengths differ by nearly the same amount. This difference and the unsymmetrical bridging of the acetato groups, together with other aspects of the crystallographic computations (vide supra), support an ordered structural model. However, a small degree of disorder involving the two metals cannot be ruled out. Indeed, the fact that the Fe–O1 bond in **4'** is significantly longer than the Fe3–O1 bond (1.943 (2) Å) in **1'** may be the consequence of the small amount of Fe/Zn disorder likely to be present in the solid-state structure of the Fe/Zn compound.

Mössbauer Properties. Mössbauer spectroscopy has been useful for ascertaining the oxidation states of the iron centers in complexes **1**–**5**, and the results for all the complexes are listed in Table VI. The Mössbauer spectrum of **1** as a crystalline solid at 55 K exhibits two quadrupole doublets of equal intensity having δ values of 0.48 and 1.13 mm/s and ΔE_Q values of 0.54 and 2.91 mm/s, respectively (Figure 2A), in agreement with the results reported by Suzuki et al. on the acetate complex.[13a] The Mössbauer parameters correspond to a high-spin Fe^{III} center and a high-spin Fe^{II} center,[34] respectively, and corroborate the crystallographic results obtained for **1**. Discrete quadrupole doublets are observed up to room temperature, suggesting that intervalence electron transfer is slow on the Mössbauer time scale ($< 10^7\ s^{-1}$) even at the highest temperature of observation. At 4.2 K, the spectra of **1** (and **2**) display magnetic hyperfine features even in zero applied magnetic field, showing that the two iron centers are spin-coupled to a state with half-integer spin. These results are similar to those found for the previously characterized mixed valence complex $[Fe^{II}Fe^{III}HXTA(OAc)_2]^{2-}$.[14] A detailed analysis of the magnetic hyperfine features found in the 4.2 K Mössbauer spectra of the $Fe^{II}Fe^{III}$ complexes will be published in a separate account.

The Mössbauer spectra of **3** and **5** reveal the presence of only one type of iron center per molecule. **3** exhibits a quadrupole

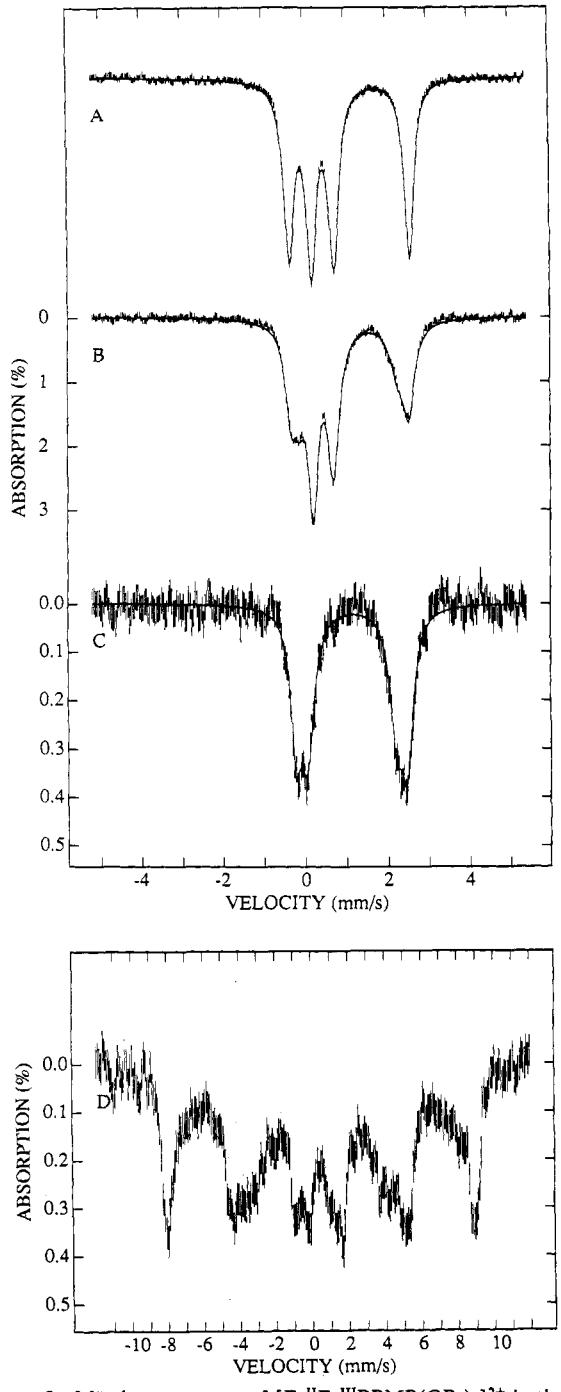

Figure 2. Mössbauer spectra of $[Fe^{II}Fe^{III}BPMP(OPr)_2]^{2+}$ in the solid state at 55 K (a) and in CH_3CN at 55 K (b), $[Fe^{II}Ga^{III}BPMP(OPr)_2]^{2+}$ in CH_3COCH_3 at 4.2 K (c), and $[Zn^{II}Fe^{III}BPMP(OPr)_2]^{2+}$ in CH_3CN at 55 K (d).

(31) (a) Hendrickson, W. A.; Co, M. S.; Smith, J. L.; Hodgson, K. O.; Klippenstein, G. L. *Proc. Natl. Acad. Sci. U. S. A.* **1982**, *79*, 6255–6259. (b) Hedman, B.; Co, M. S.; Armstrong, W. H.; Hodgson, K. O.; Lippard, S. J. *Inorg. Chem.* **1986**, *25*, 3708–3711.

(32) Maroney, M. J.; Kurtz, D. M., Jr.; Nocek, J. M.; Pearce, L. L.; Que, L., Jr. *J. Am. Chem. Soc.* **1986**, *108*, 6871–6879.

(33) Shannon, R. D.; Prewitt, C. T. *Acta Crystallogr.* **1969**, *B25*, 925.

Table VI. Mössbauer Properties of the Binuclear Complexes

complex	T, K	solvent	δ^a	%Fe	$\Delta E_Q{}^a$	Γ^a
$[Fe_2BPMP(OPr)_2](BPh_4)_2$	55	solid	1.13	48	2.91	0.29
			0.48	52	0.54	0.30
	203	solid	1.06	48	2.35	0.31
			0.44	52	0.51	0.28
	300	solid	0.96	51	1.83	0.38
			0.41	49	0.53	0.28
$[Fe_2BPMP(OPr)_2](BPh_4)_2$	55	CH_3CN	1.12	25	2.85	0.31
			1.10	25	2.39	0.44
			0.48	50	0.49	0.32
$[Fe_2BPMP(OAc)_2](BF_4)_2{}^c$	77	solid	1.16	49	2.42	0.41
			0.47	51	0.51	0.33
$[Fe_2BPMP(OBz)_2](PF_6)_2$	55	CH_3COCH_3	1.12	25	2.85	0.31
			1.10	25	2.39	0.44
			0.48	50	0.49	0.32
$[Fe_2BPMP(OBz)_2](BF_4)_2{}^c$	77	solid	1.15	50	2.06	0.56
			0.56	50	0.47	0.28
$[Fe^{II}Ga^{III}BPMP(OPr)_2](BPh_4)_2$	4.2	CH_3COCH_3	1.17	56	2.20	0.40
			1.16	44	2.75	0.31
$[Fe_2HXTA(OAc)_2]^{2-}$	55	solid	1.23	53	2.81	0.28
			0.51	47	0.46	0.34
reduced uteroferrin[b]	119	aqueous	1.22	52	2.63	0.32
			0.53	48	1.78	0.35
reduced uteroferrin–PO_4[b]	119	aqueous	1.23	50	2.76	0.34
			0.54	50	0.78	0.34

[a] Units of mm/s; isomer shifts relative to Fe metal at room temperature. [b] Data from: Pyrz, J. W.; Sage, J. T.; Debrunner, P. G.; Que, L., Jr. *J. Biol. Chem.* **1986**, *261*, 11015–11020. [c] From ref 13a.

doublet with δ and ΔE_Q values of 1.17 and 2.53 mm/s, respectively (Figure 2C), typical of high-spin Fe^{II} and similar to those found for the Fe^{II} center of **1**. **5**, on the other hand, displays magnetic hyperfine interactions even at 200 K, which is characteristic of mononuclear Fe^{III} with a long electron spin–lattice relaxation time.

The Mössbauer spectra of these complexes in solution in general correspond to the solid-state spectra with one difference. The quadrupole doublets associated with the Fe^{II} sites in **1**–**3** have larger line widths in the solution spectra and can be fit with two sets of δ and ΔE_Q values (B and C of Figure 2). The heterogeneity in the Fe^{II} sites may reflect the differences in the sites designated as Fe2 and Fe3 in the structure of **1′**. In the crystal, the ferrous center occupies the Fe2 site, and the ferric center occupies the Fe3 site, thus giving rise to the Mössbauer spectrum in Figure 2A. The solid-state restraints are lifted in solution, allowing both Fe2 and Fe3 sites to be half-occupied by the Fe^{II} center. Since the Fe2 and Fe3 sites are not identical, 50% occupancy by the Fe^{II} center at each site could give rise to the observed heterogeneity. The Fe^{III} center should in principle also reflect this solution heterogeneity, but the Fe^{III} parameters are less sensitive to small differences in the environment.[34]

NMR Studies. NMR spectroscopy has also proven to be a useful technique in characterizing the mixed valence complexes. As illustrated in Figure 3A, the ^1H NMR spectrum of **1** consists of relatively sharp resonances that span 400 ppm in chemical shift. The narrow line widths of the signals are consistent with the presence of a high-spin Fe^{II} center in the molecule, with the diiron(II,III) complex adopting the T_{1e} of the faster relaxing ferrous ion.[35] The spectrum of **1** resembles the results obtained for the mixed valence complex of HXTA, showing that sharp, downfield-shifted signals are characteristic of this class of $Fe^{II}Fe^{III}$ complexes;[14] the ^1H NMR spectrum of the analogous $[Fe^{II}Fe^{III}HXTA(OPr)_2]^-$ is shown in Figure 3B for comparison. Using the assignments of the signals for $[Fe^{II}Fe^{III}HXTA(OPr)_2]^-$, along with T_1 and ligand substitution experiments on **1**, we have been able to assign all the resonances in **1**. While we can account for all the protons in **1**, analysis of the assignments reveals that only 16 distinct signals are observed for the $BPMP^-$ ligand, indicating that electron transfer between the metal centers is fast

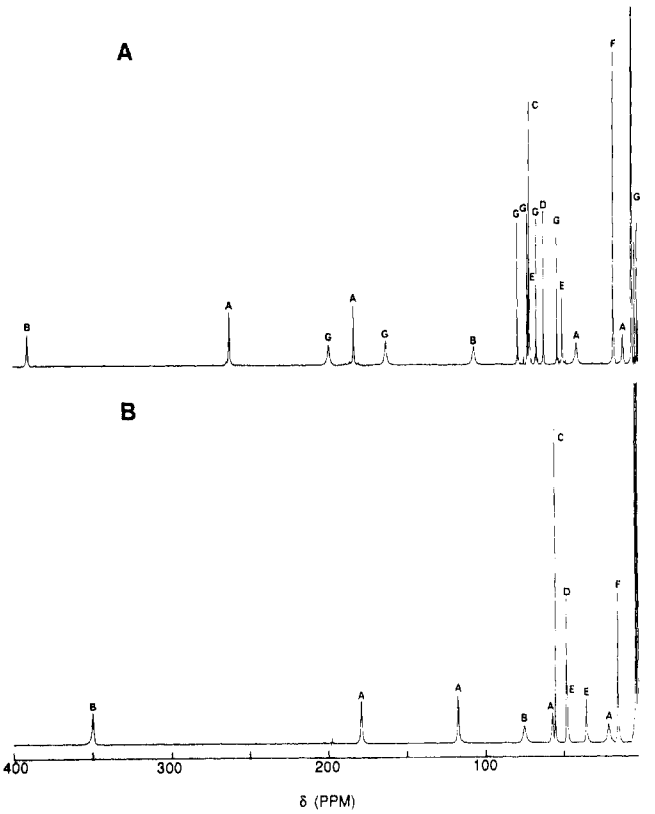

Figure 3. ^1H NMR spectra of (a) $[Fe^{II}Fe^{III}BPMP(OPr)_2]^{2+}$ in CD_3COCD_3 and (b) $[Fe^{II}Fe^{III}HXTA(OPr)_2]^{2-}$ in CD_3OD with 0.050 M $NaO_2Pr/HOPr$. Assignments (integration): (A) NCH_2py (2); (B) NCH_2Ar (2); (C) *p*-$ArCH_3$ (3); (D) *m*-ArH (2); (E) $^-OPrCH_2$ (2); (F) $^-OPrCH_3$ (6); (G) pyH (2). Ar and py refer to the phenolate and pyridine moieties, respectively.

on the NMR time scale.[36] In addition, the CH_2 protons of the bound propionates are diastereotopic, with signals found at 51 and 72 ppm, implying the absence of an improper rotation axis in the molecule. Taken together, these results are consistent with **1** retaining in solution the triply bridged diiron core that was found in the solid-state structure.

The large span of shifts observed for the $Fe^{II}Fe^{III}$ complexes suggests that the antiferromagnetic interaction between the two metal ions is weak. Indeed the temperature dependence of the shifts (data not shown) allow us to estimate that $-2J < 10$ cm^{-1} ($\mathcal{H} = -2JS_1S_2$). A more accurate determination cannot be made using this technique because of the potential variations in A_H as a function of S′ states and the difficulty in assessing the dipolar contribution of the Fe^{II} center.[35] However, the magnitude of $-2J$ compares favorably with the values (6–16 cm^{-1}) reported by Suzuki et al.[13a,b] on related compounds.

We have also obtained the ^1H NMR spectra of the heterobimetallic complexes **3**–**5**. The spectra clearly reflect the difference in the oxidation state of the iron in the $Zn^{II}Fe^{III}$ and $Fe^{II}Ga^{III}$ complexes. The spectra of $Zn^{II}Fe^{III}$ complexes **4** and **5** consist of poorly resolved resonances and are significantly broader than the signals found in either the diiron(II,III) complexes or the $Fe^{II}Ga^{III}$ complex **3**. For comparison, the line widths at half-height for **5** range from 450 to 1200 Hz, while the range for **3** is 90–450 Hz. This difference in line widths arises from differences in T_{1e} values ($\approx 10^{-12}$ s for Fe^{II} and $\approx 10^{-9}$–10^{-10} s for Fe^{III}), so the relevant correlation time for the Fe^{II}-containing complexes is T_{1e} and that for **4** and **5** is τ_R ($\approx 10^{-11}$ s).[37] The sharpness of the signals in the spectrum of **3** has allowed us to observe all the protons in the molecule, while only *p*-cresol and some of the pyridyl protons of

(34) Greenwood, N. N.; Gibb, T. C. *Mössbauer Spectroscopy*; Chapman and Hall: London, 1971; pp 113–168.

(35) Bertini, I.; Luchinat, C. *NMR of Paramagnetic Molecules in Biological Systems*; Benjamin/Cummings: Menlo Park, California, 1986.

(36) If electron transfer were slow on the NMR time scale, we would expect to observe 37 distinct signals.

(37) T_{1e} values for magnetically dilute ferrous complexes are $\approx 10^{-12}$ s while those of ferric complexes range from 10^{-9} to 10^{-11} s.

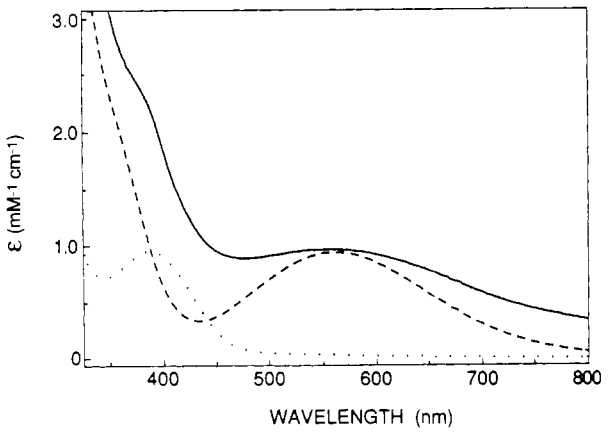

Figure 4. Visible absorption spectra of (—) $[Fe^{II}Fe^{III}BPMP(OPr)_2]^{2+}$, (···) $[Fe^{II}Ga^{III}BPMP(OPr)_2]^{2+}$, and (---) $[Zn^{II}Fe^{III}BPMP(OPr)_2]^{2+}$ in CH_3CN at ambient temperature.

Table VII. Electrochemical and Visible Absorption Properties of the Binuclear Complexes[a]

complex	$E_{1/2}$[b]	ΔE_p[b]	i_c/i_a[c]	λ_{max}[d] (ϵ[e])
$[Fe_2BPMP(OPr)_2](BPh_4)_2$	−10	60	1.02	390 (sh, 2200)
	692	68	*f*	554 (950)
$[Fe_2BPMP(OAc)_2](BF_4)_2$[g]	−30	70	1.0	556 (900)
	680	70	1.0	
$[Fe_2BPMP(OBz)_2](PF_6)_2$	60	60	1.03	375 (sh, 3300)
	750	60	0.98	580 (930)
$[Fe_2BPMP(OBz)_2](BF_4)_2$[g]	50		1.0	575 (970)
	730		1.0	
$[GaFeBPMP(OPr)_2](BPh_4)_2$	587	60	0.85	387 (980)
$[FeZnBPMP(OAc)_2](BPh_4)_2$	−4	59	1.02	552 (850)
$[FeZnBPMP(OPr)_2](BPh_4)_2$	−19	60	1.02	562 (920)

[a] In CH_3CN. [b] Units of mV. [c] i_c/i_a = 1.02 for the ferricinium/ferrocene couple at the same experimental conditions employed. [d] Units of nm. [e] Units of M^{-1} cm^{-1}. [f] The large anodic peak of BPh_4^- prevents accurate determination of the height of i_a. [g] From ref 13a.

$BPMP^-$ are found in the spectra of **4** and **5**.

Electronic Absorption Properties. The absorption data for all the complexes are found in Table VII, and the visible absorption spectra in acetonitrile for the bis(propionate) complexes **1**, **3**, and **5** are displayed in Figure 4. The spectrum of **1** contains two components: a shoulder at 385 nm and a broad absorption band at 554 nm. Comparisons of this spectrum with those of **3** and **5** allow us to obtain a qualitative understanding of the nature of these transitions. The absorption spectrum of **3** consists of a single band centered at 387 nm, which is at an energy similar to the high-energy shoulder found in **1**. These bands are undoubtedly a result of the presence of the ferrous center in the complexes; they are tentatively assigned as Fe^{II}-to-pyridine charge-transfer transitions.

The low-energy absorption feature in **1** is also present in the spectrum of **5** at 562 nm. We have assigned these bands as phenolate-to-Fe^{III} charge-transfer transitions. To corroborate this assignment, we have probed these bands by resonance Raman spectroscopy. Since the geometry about the ferric centers is nearly the same in **1** and **5**, we would expect to observe similar resonance Raman spectra if our assignment is correct. Laser excitation of **1** and **5** at 615 and 593 nm, respectively, in CD_3CN produced identical resonance-enhanced Raman spectra with bands at 1168, 1198, 1258, 1320, 1482, and 1616 cm^{-1}. These vibrations are observed in other metal–phenolate complexes and correspond to phenolate deformation modes.[38] These comparisons illustrate how **3** and **5** have allowed us to further understand the physical properties of the diiron(II,III) complexes.

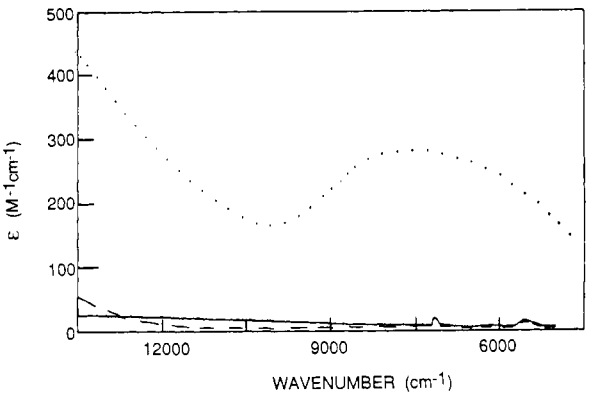

Figure 5. Near-IR spectra of (···) $[Fe^{II}Fe^{III}BPMP(OPr)_2]^{2+}$, (—) $[Fe^{II}Ga^{III}BPMP(OPr)_2]^{2+}$, and (---) $[Zn^{II}Fe^{III}BPMP(OPr)_2]^{2+}$ in CD_3CN at 22 K.

As shown in Figure 5 for **1**, the diiron(II,III) complexes have an additional broad absorption band in the near-IR region, a feature also observed for previously reported complexes analogous to **1**. These features are assigned as metal–metal charge-transfer transitions or intervalence transfer (IT) absorption bands. Also included in Figure 5 are the absorption spectra for **3** and **5**, which exhibit no features in this region and thus support the assignment of these near-IR bands in **1** and **2** as IT transitions. The properties associated with these IT bands for **1** and **2** are collected in Table VIII. While the following discussion is focused on **1**, the same arguments can be applied to **2**. For **1**, the energy of the optical transition (E_{OP}) for the near-IR peak is 7420 cm^{-1}, and the bandwidth at half-height ($\Delta\nu_{1/2}$) is 5290 cm^{-1} as determined from a Gaussian fit of the band (see Experimental Section). The value for $\Delta\nu_{1/2}$ is larger than the theoretical value of 4140 cm^{-1} predicted by eq 1.[39] In fact, the ratio of $\Delta\nu_{1/2}(obsd)/\Delta\nu_{1/2}(theor)$ = 1.3

$$\Delta\nu_{1/2} = (2.31 \times 10^3 E_{OP})^{1/2} \quad (1)$$

is commonly found for weakly to moderately coupled binuclear mixed valence dimers.[40] The extent of electron delocalization of the excess electron from Fe^{II} to Fe^{III} in the ground state is given by eq 2,[39] where ϵ_{max} is the molar extinction coefficient at E_{OP}

$$\alpha^2 = 4.2 \times 10^{-4} \epsilon_{max} \Delta\nu_{1/2} / E_{OP} d^2 \quad (2)$$

in M^{-1} cm^{-1}, and d is the distance between the two metal ions in Å. Using the Fe–Fe distance of 3.365 Å that was determined by the X-ray analysis of **1**, we obtain a value of $\alpha^2 = 8.2 \times 10^{-3}$. In addition, first-order perturbation theory shows that the resonance energy matrix element, V_{ab}, can be calculated from the relationship, $V_{ab} = \alpha E_{OP}$,[39] to yield V_{ab} = 670 cm^{-1} (1.9 kcal/mol).

Analysis of properties of the IT bands also allows us to explore the kinetics of electron transfer.[41] From a quantum mechanical treatment,[42] the following expression is derived for the thermal rate constant for electron transfer:

$$k_{et} = \nu_{et} \exp[-\Delta G^*/RT] \quad (3)$$

where the preexponential term, ν_{et}, is the frequency factor for electron transfer and in the high-temperature limit can be described as

$$\nu_{et} = 2\pi^{3/2} V_{ab} / h(kTE_{OP})^{-1/2} \quad (4)$$

and ΔG^*, the thermal free energy of electron transfer, is $E_{OP}/4 - V_{ab}$ for a symmetrical mixed valence complex.[43] The calculated value of k_{et} for **1** using eq 3 is 2.4×10^{12} s^{-1}, and a similar value for k_{et} of 2.3×10^{12} s^{-1} is found for **2**. These values are greater

Table VIII. Near-IR Properties of the Mixed Valence Diiron Complexes[a]

complex	E_{OP}[b] (ϵ[c])	ΔG^*[d]	$\Delta\nu_{1/2}$[b]	α^2	k_{et}[e]
$[Fe_2BPMP(OPr)_2](BPh_4)_2$	7420 (310)	3.38	5290 (4140)	0.0082	2.4×10^{12}
$[Fe_2BPMP(OBz)_2](PF_6)_2$	7330 (290)	3.37	5430 (4120)	0.0080	2.3×10^{12}

[a] In CD_3CN. [b] Units of cm^{-1}. [c] Units of M^{-1} cm^{-1}. [d] Units of kcal/mol. [e] Units of s^{-1}.

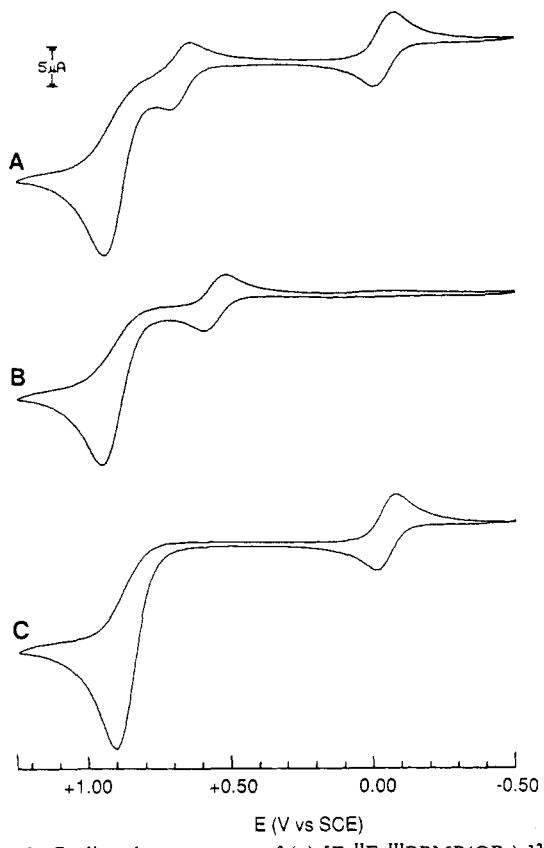

Figure 6. Cyclic voltammograms of (a) $[Fe^{II}Fe^{III}BPMP(OPr)_2]^{2+}$, (b) $[Fe^{II}Ga^{III}BPMP(OPr)_2]^{2+}$, and (c) $[Zn^{II}Fe^{III}BPMP(OPr)_2]^{2+}$ versus SCE in CH_3CN with 0.1 M $TBABF_4$ under N_2 at a 100 mV/s scan rate. The irreversible oxidative waves near +900 mV are due to the oxidation of the BPh_4 anion.

than for most binuclear d^5,d^6 mixed valence species. Creutz has pointed out that, in a series of mixed valence $[Ru(bpy)_2Cl]_2L$ complexes (where L is the bridging ligand), there is a 100-fold increase in k_{et} from 10^7 to 10^9 s^{-1} as the metal–metal distance decreases from ~14 to ~7 Å.[39] Using this trend as a qualitative guide, it is not surprising that the values obtained for the k_{et} of **1** and **2** are $\sim 10^{12}$, since the triply bridged diiron units have relatively short Fe–Fe distances of ~3.4 Å.

Finally, the above optical results and analyses of the IT bands show that **1** and **2** are weakly to moderately coupled mixed valence species. These complexes are therefore assigned as type II mixed valence species in the classification scheme developed by Robin and Day.[44]

Electrochemistry. The observations made during the synthesis of **1**–**3** suggested that redox processes were involved in their formation. We have further investigated the redox properties of these complexes by cyclic voltammetry and controlled potential coulometry. The results of the cyclic voltammetry experiments are found in Table VII, and the cyclic voltammograms (CV) for **1**, **3**, and **5** are displayed in Figure 6. In acetonitrile with $TBABF_4$ as the supporting electrolyte, **1** exhibited two reversible one-electron waves at +692 and −10 mV versus SCE, which correspond to the $Fe^{III}Fe^{III}/Fe^{II}Fe^{III}$ and $Fe^{II}Fe^{III}/Fe^{II}Fe^{II}$ couples, respectively, in agreement with the observations of Suzuki et al. on the acetate complex.[13a] Similar results were obtained for **2**, with the two couples being shifted to more positive potentials by 58 and 70 mV, respectively. For **3**, where Ga^{III} was substituted for Fe^{III}, only a high potential Fe^{III}/Fe^{II} couple is observed at +587 mV versus SCE. When Zn^{II} was substituted for Fe^{II}, a single Fe^{III}/Fe^{II} couple was observed (−19 mV versus SCE in **5**). All the measured iron couples approach chemical reversibility as gauged by (i) their ΔE_p values being centered around 60 mV, (ii) their $E_{1/2}$ values being independent of scan rates from 50 to 200 mV/s, and (iii) each couple having cathodic and anodic waves of equal height (i.e., $i_c/i_a \approx 1$).[45]

The CV results for the heterobimetallic complexes clearly illustrate the significant effects the oxidation state of the second metal ion has on the redox potential at the iron center. The $E_{1/2}$ value for the Fe^{III}/Fe^{II} couple in **3**, which contains the trivalent gallium ion, was ca. 600 mV more positive than found for the corresponding couple in **5**. This difference suggests that, for these heterobimetallic complexes, electrostatic interactions are important in determining the potential of the system, while electron delocalization through the triply bridged metal core makes relatively small contributions. It would appear that the ligand framework (i.e., $BPMP^-$ and the two carboxylates) stabilizes a binuclear center with a total charge of +5. This preference is observed not only for the complexes discussed in this paper but for the Mn_2,[30a] Fe/Mn,[19] and Fe/Cu[19] derivatives as well.

The thermodynamic stability of the diiron(II,III) complexes **1** and **2** can be estimated by examining the comproportionation equilibrium

$$[Fe^{II}Fe^{II}(BPMP)X_2]^+ + [Fe^{III}Fe^{III}(BPMP)X_2]^{3+} \underset{}{\overset{K_{com}}{\rightleftharpoons}} 2[Fe^{II}Fe^{III}(BPMP)X_2]^{2+} \quad (5)$$

$$\Delta E = (RT/nF) \ln K_{com} \quad (6)$$

where X is OPr^- or OBz^-. As discussed above, **1** and **2** show two sequential reductions (Figure 6A), separated by an amount $\Delta E = E_1 - E_2$, where E_1 and E_2 correspond to the $Fe^{III}Fe^{III}/Fe^{II}Fe^{III}$ and $Fe^{II}Fe^{III}/Fe^{II}Fe^{II}$ couples, respectively. Equation 6 demonstrates that the thermodynamic significance of ΔE is its relationship to K_{com}, the comproportionation equilibrium constant. Large values of ΔE indicate substantial stability of the diiron(II,III) ion over its corresponding diiron(III,III) and diiron(II,II) species. For **1** and **2**, the values for ΔE are 702 and 690 mV, which yields K_{com} values of 7.5×10^{11} and 4.7×10^{11}, respectively.

As discussed by Gagnē and co-workers,[46] K_{com} is dependent on several factors, the most relevant for the present study being (i) structural effects that occur upon reduction, (ii) Coulombic interactions, (iii) magnetic exchange effects, and (iv) electron delocalization which enhances the stability of the mixed valence species. It is therefore instructive to compare the reduction potentials of **1** with its corresponding heterobimetallic bis(propionate) complexes **3** and **5**, to further investigate some of these factors. As already discussed, the heterobimetallic complexes have many of the same structural and Coulombic features as found in **1**, including (i) triply bridged binuclear metal ion units, (ii) similar octahedral metal ion coordination and metal–metal distances, and (iii) the same overall positive divalent charge. Thus, within this series of binuclear complexes, structural effects and Coulombic interactions should be constant. In addition, magnetic exchange effects, which are not present in **3** and **5**, are small in **1**. The electrochemical experiments should then allow us to determine if electron delocalization is the important factor in stabilizing the mixed valence species.

To examine the role of electron delocalization in stabilizing the diiron(II,III) complexes, we have compared the reductive processes in **1** to those found in **3** and **5**. Specifically, we have compared E_1 to the $E_{1/2}$ value of **3**, since they both measure the Fe^{III}/Fe^{II} reduction in a fully oxidized binuclear(III,III) species. Similarly, comparison of E_2 and the $E_{1/2}$ value of **5** is appropriate because

(38) Pyrz, J. W.; Roe, A. L.; Stern, L. J.; Que, L., Jr. *J. Am. Chem. Soc.* **1985**, *107*, 614–620.
(39) Hush, N. S. *Prog. Inorg. Chem.* **1967**, *8*, 391–444.
(40) Powers, M. J.; Meyer, T. J. *J. Am. Chem. Soc.* **1979**, *100*, 6284–6286.
(41) Meyer, T. J. *Chem. Phys. Lett.* **1979**, *64*, 417–420.
(42) (a) Hopfield, J. J. *Proc. Natl. Acad. Sci. U. S. A.* **1974**, *71*, 3640. (b) Kestner, N. R.; Logan, J.; Jortner, J. *J. Phys. Chem.* **1974**, *78*, 2148.
(43) Creutz, C. *Prog. Inorg. Chem.* **1983**, *30*, 1–73.
(44) Robin, M. B.; Day, P. *Adv. Inorg. Chem. Radiochem.* **1967**, *10*, 247–422.
(45) Bard, A. J.; Falkner, L. R. *Electrochemical Methods*; Wiley: New York, 1983.
(46) Gagnē, R. R.; Spiro, C. L.; Smith, T. J.; Hamann, C. A.; Thies, W. R.; Shiemke, A. K. *J. Am. Chem. Soc.* **1981**, *103*, 4073–4081.

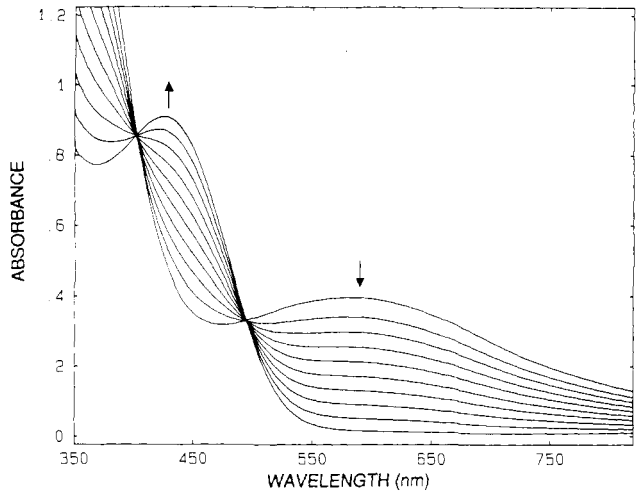

Figure 7. Spectral change of $[Fe^{II}Fe^{III}BPMP(OBz)_2]^{2+}$ during a controlled potential coulometry experiment in CH_3CN with $E = -300$ mV versus Ag/AgCl.

they examine the Fe^{III}/Fe^{II} reduction of the species, $[Fe^{III}M^{II}BPMP(OPr)_2]^{2+}$ (where M^{II} is a divalent cation) to their fully reduced counterparts. If electron delocalization were the dominant factor in stabilizing the mixed valence state, we would expect $E_1 > E_{1/2}$ for **3** and $E_2 < E_{1/2}$ for **5**. Examination of the electrochemical results shows that, while **1** is indeed easier to reduce than **3** (by 105 mV or 2.4 kcal/mol), the reduction potential for the ferric center in **5** is essentially the same as E_2. Furthermore, the related heterobimetallic complexes, $[Fe^{III}Mn^{II}BPMP(OPr)_2]^{2+}$ and $[Fe^{III}Cu^{II}BPMP(OPr)_2]^{2+}$, also have similar $E_{1/2}$ values (24 and 6 mV versus SCE, respectively), for their Fe^{III}/Fe^{II} couples.[19] These results show that the Fe^{III}/Fe^{II} reduction potentials in the $[Fe^{III}M^{II}BPMP(OPr)_2]^{2+}$ complexes are independent of the second metal ion, an observation that is inconsistent with electron delocalization being the dominant factor in the stabilization of the diiron(II,III) complexes. While electron delocalization in the mixed valence form probably has some role in the stability of **1**, as indicated by the 105-mV difference between E_1 and $E_{1/2}$ for **3**, it cannot be the major influence toward the formation of **1**. Other factors, such as the strong oxidizing ability of the $Fe^{III}Fe^{III}$ species, most likely contribute to the formation of the mixed valence complex over its more oxidized and reduced counterparts. The results of this comparison point out the importance of examining both redox couples in determining the effects that various factors have on K_{com}. This is particularly crucial when evaluating the role that electron delocalization has in stabilizing binuclear mixed valence complexes.

We have used controlled potential coulometry (CPC) to further explore the accessibility of the $Fe^{II}Fe^{II}$ and $Fe^{III}Fe^{III}$ analogues of the diiron(II,III) complexes. At a potential of −300 mV versus Ag/AgCl, CPC experiments measured 1.05 e^-/mol of **2**, which agrees with the assignment of E_2 being associated with the reversible one-electron reduction of **2**. This reaction has been followed spectrophotometrically, and as illustrated in Figure 7, **2** is cleanly converted to the diiron(II,II) species. The loss of the LMCT band of **2** at 580 nm parallels the appearance of a new feature at 424 nm, which is assigned to the diiron(II,II) complex. We have synthesized $[Fe^{II}Fe^{II}BPMP(OPr)_2]^+$,[18] which also has an absorption band in this region (441 nm) and thus supports the association of the 424-nm band with the diiron(II,II) species. (We attribute the difference in the absorption maxima to the effect of benzoate versus propionate bridges.) While the CV experiments show that E_1 is reversible, we have not been able to obtain accurate coulometric data for this redox couple, probably due to the instability of the $Fe^{III}Fe^{III}$ species under the conditions of the CPC experiment. However, Suzuki et al. recently reported the synthesis of $[Fe^{III}Fe^{III}BPMP(OBz)_2](ClO_4)_3$, demonstrating that the diferric species can be stabilized under appropriate conditions.[13d]

EPR Spectroscopy. EPR spectroscopy has been useful for characterizing diiron(II,III) centers in the binuclear iron–oxo proteins.[2,4a,4d,5] As stated earlier, these centers exhibit signals with $g_{av} < 2$, which is indicative of antiferromagnetic coupling of a high-spin (^6A state) Fe^{III} ion to a high-spin (^5T state) Fe^{II} ion, resulting in an $S = {}^1/_2$ ground state. A similar signal at $g_{av} = 1.92$ is reported for the mixed valence complex derived from the reduction of $[Fe_2(Me_3TACN)_2O(OAc)_2]^{2+}$.[15] We reported earlier that the present diiron(II,III) complexes and the analogous $[Fe_2HXTA(OAc)_2]^{2-}$ did not exhibit such signals under similar conditions.[14,18] However, subsequent examinations of **1** at low temperature (2.2 K) and high modulation amplitude (40 G) revealed broad, high-field features centered near $g = 1.6$ (Figure 8A) with weak, low-field features observed at $g = 10.1$ and 7.6. A similarly broad, high-field signal near $g = 1.7$ has been found by Suzuki et al.[13a] for the corresponding acetate complex. That these signals arise from the mixed valence complex **1** is supported by their absence in the EPR spectra of **3** and **5**. Complex **3** exhibits a weak integer spin EPR signal at low field,[47] while complex **5** exhibits sharp signals at $g = 9$ and 4.3, as is typical of an $S = {}^5/_2$ system in the rhombic limit (Figure 8B). The EPR properties of **1** are unique and not fully understood at present; they probably reflect the complexities of a system where the antiferromagnetic coupling between the iron centers is weak and comparable to the zero field splitting of the Fe^{II} site,[48] and more detailed studies of the magnetic and Mössbauer properties of **1–5** are in progress.

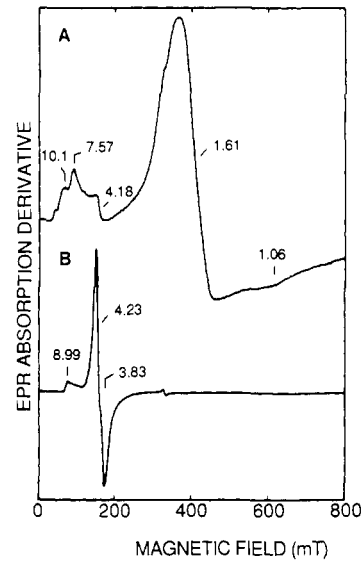

Figure 8. EPR spectra of (a) $[Fe^{II}Fe^{III}BPMP(OPr)_2]^{2+}$ in CH_3CN under N_2 (experimental conditions: 4.1×10^{-3} M, temperature, 2.3 K; gain, 2.5×10^3; modulation amplitude, 40 G; frequency, 9.197 GHz; power, 0.2 mW) and (b) $[Zn^{II}Fe^{III}BPMP(OPr)_2]^{2+}$ in CH_3CN/toluene under N_2 (experimental conditions: 4.5×10^{-4} M, temperature, 2.2 K; gain, 6.3×10^3; modulation amplitude, 40 G; frequency, 9.188 GHz; power, 0.2 mW).

The EPR properties of **1** and **2** are particularly relevant to the case of the phosphate complex of reduced uteroferrin, the purple acid phosphatase from porcine uterus. The readily observable EPR spectrum of reduced uteroferrin is obliterated upon addition of phosphate, and only under conditions of high power, large modulation amplitude, and temperatures below 8 K (conditions similar to those used for **1** and **2**) can the broad anisotropic signal be observed.[48] Magnetic studies of the phosphate complex show that $-2J = 6.0 \pm 0.5$ cm^{-1} compared to $-2J = 19.8 \pm 0.5$ cm^{-1} for reduced uteroferrin. These differences in the antiferromagnetic coupling between the Fe^{II} center and the Fe^{III} center may be the key to the peculiar spectroscopic properties, and the complexes discussed herein can serve to test emerging hypothetical models that explain these properties.

(47) Hendrich, M. P., unpublished observations.
(48) Day, E. P.; David, S. S.; Peterson, J.; Dunham, W. R.; Bonvoisin, J. J.; Sands, R. H.; Que, L., Jr. *J. Biol. Chem.* **1988**, *263*, 15561–15567.

Summary and Perspectives. We have synthesized and characterized $Fe^{II}Fe^{III}$ complexes of the binucleating ligand BPMP, which serve as models for the mixed valence oxidation state in binuclear iron–oxo proteins such as hemerythrin, methane monooxygenase, and purple acid phosphatase. These complexes exhibit novel Mössbauer, EPR, NMR, magnetic, and electronic spectral properties, which contribute to our understanding of the mixed valence sites in proteins. In addition, we have discovered a general method for obtaining heterobimetallic complexes containing iron in one of the metal sites. The $Zn^{II}Fe^{III}$ and $Fe^{II}Ga^{III}$ complexes, in particular, will be useful for determining the properties of the isolated iron centers in the absence of antiferromagnetic coupling and will thus aid in unraveling the complexities of the $Fe^{II}Fe^{III}$ interaction that give rise to their novel Mössbauer, EPR, and magnetic properties. Furthermore, the $Zn^{II}Fe^{III}$ complex and other $M^{II}Fe^{III}$ complexes that can be synthesized by similar procedures may also serve as useful models for the $M^{II}Fe^{III}$ forms of the purple acid phosphatases[49–53] and the $Cu^{II}Fe^{III}$ center in cytochrome oxidase.[54]

Acknowledgment. We thank Prof. J. D. Britton for his generous help in solving the structure of the mixed valence complex and Carlos Juarez-Garcia for his assistance in some of the Mössbauer experiments. This work has been supported by the National Institutes of Health through Grants GM-38767 (L.Q.), GM-22701 (Eckard Münck), and GM-30306 (O.P.A.) and an NIH postdoctoral fellowship for A.S.B. (GM-11533). The Nicolet R3m/E X-ray diffractometer and computing system at Colorado State University was purchased with funds provided by the National Science Foundation.

Note Added in Proof. Recently, Buchanan, Hendrickson, and co-workers reported a complex similar to **1**, with *N*-methylimidazole ligands instead of pyridines, that exhibits valence detrapping at temperatures above 100 K (*J. Am. Chem. Soc.* **1989**, *111*, 2745–2746).

Supplementary Material Available: Tables of atomic positional parameters and their estimated standard deviations, general thermal parameters, and complete bond lengths and bond angles for **1′** and **4′** (30 pages); tables of calculated and observed structure factors (105 pages). Ordering information is given on any current masthead page.

(49) Beck, J. L.; Keough, D. T.; de Jersey, J.; Zerner, B. *Biochim. Biophys. Acta* **1984**, *791*, 357–363.
(50) Beck, J. L.; McConachie, L. A.; Summors, A. C.; Arnold, W. N.; de Jersey, J.; Zerner, B. *Biochim. Biophys. Acta* **1986**, *869*, 61–68.
(51) Beck, J. L.; de Jersey, J.; Zerner, B.; Hendrich, M. P.; Debrunner, P. G. *J. Am. Chem. Soc.* **1988**, *110*, 3317–3318.
(52) Davis, J. C.; Averill, B. A. *Proc. Natl. Acad. Sci. U. S. A.* **1982**, *79*, 4623–4627.
(53) Beck, J. L.; McArthur, M. J.; de Jersey, J.; Zerner, B. *Inorg. Chim. Acta* **1988**, *153*, 39–44.
(54) Brudvig, G. W.; Stevens, T. H.; Morse, R. H.; Chan, S. I. *Biochemistry* **1981**, *20*, 3912–3921.

Photodissociation of Cyclopentadienyliron(II) Arene Cations: Detection and Characterization of Reactive Intermediates by Means of Time-Resolved Laser Spectroscopy

Douglas R. Chrisope, Kyung Mi Park, and Gary B. Schuster*

Contribution from the Department of Chemistry, University of Illinois, Roger Adams Laboratory, Urbana, Illinois 61801. *Received January 17, 1989*

Abstract: Cyclopentadienyliron(II) arene cations ($[CpFeArH]^+$) exist in solution as a mixture of freely solvated ions and as ion pairs with an anionic counterion (X^-). Irradiation of either the free ion or the ion pair in solutions containing benzonitrile (PhCN) leads to loss of the arene ligand and formation of a tris-nitrile complex ($[CpFe(PhCN)_3]^+$). Two important reactive intermediates are detected by time-resolved laser spectroscopy. One, formed from irradiation of the ion pair, is assigned as the ring-slipped η^4-arene–Cp–iron compound covalently bound to its counterion. The other, formed from irradiation of freely solvated cations, is assigned as the coordinatively unsaturated ring-slipped Cp–iron–η^4-arene compound. The role of these intermediates in the ligand-exchange reaction was examined.

Irradiation of an organometallic compound with light often leads to chemical processes that are not observed under thermal reaction conditions. Such is the case for the cationic (cyclopentadienyl)(arene)iron(II) complexes $[(CpFeArH)^+X^-]$. These readily prepared compounds[1] are stable in the dark but undergo efficient dearylation when exposed to light. The investigation of this reaction was focused at first on its synthetic applications.[2] However, these materials have recently taken on special significance. Meier and Zweifel report that certain $[CpFeArH]^+X^-$ complexes are highly efficient, visible-light-sensitive photoinitiators for the polymerization of epoxides.[3] Since only a few compounds

Chart I

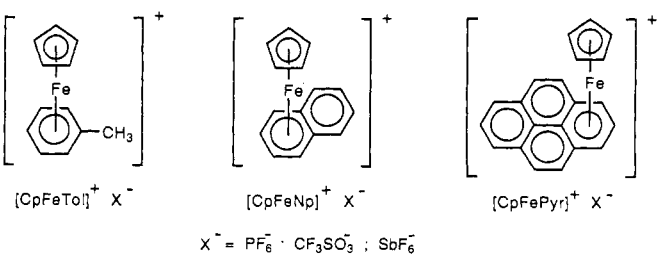

are known to have properties satisfactory for application in this area, it is important to probe in detail the mechanism of photodearylation and its connection to the photoinitiation of polymerization.

The electronic structure of $[CpFeArH]^+X^-$ complexes was investigated by Hendrickson and co-workers.[4] They showed by

(1) Sutherland, R. G. *J. Organomet. Chem. Libr.* **1976**, *3*, 311. Green, M. L. H.; Pratt, L.; Wilkinson, G. *J. Chem. Soc. A* **1960**, 989.
(2) Gill, T. P.; Mann, K. R. *Inorg. Chem.* **1980**, *19*, 3007.
(3) Meier, K.; Zweifel, H. *J. Imaging Sci.* **1986**, *30*, 174. Roloff, A.; Meier, K.; Riediker, M. *Pure Appl. Chem.* **1986**, *9*, 1267. Klingert, B.; Riediker, M.; Roloff, A. *Comments Inorg. Chem.* **1988**, *7*, 109.

0002-7863/89/1511-6195$01.50/0